E-ELT PROGRAMME

MICADO Phase A
Scientific Analysis Report

Document: E-TRE-MCD-561-0007

Issue: 2.0

Date: 19.10.2009

	Name	Date & Signature
Author(s)	A. Renzini et al.	
Proj. Manager	R. Davies	

CHANGE RECORD

ISSUE	DATE	SECTION/PAGE AFFECTED	REASON/ REMARKS
1		All	First issue
1.1	22.12.08	Document Name, Sec 1	Updated according to RIXs 2 and 35 from Phase A1 review
2.0	15.10.09	All sections	General revision of text and figs, added details on some optional modes

TABLE OF CONTENTS

CONTRIBUTING AUTHORS **6**

1 SCOPE **6**

2 APPLICABLE AND REFERENCE DOCUMENTS **6**

2.1 APPLICABLE DOCUMENTS 6
2.2 REFERENCE DOCUMENTS 6

3 SCIENCE CASES **7**

3.1 THE GALACTIC CENTER 8
3.1.1 Outstanding Questions *8*
3.1.2 Science drivers and capabilities of MICADO at the EELT *10*
3.1.3 Instrument Requirements *13*
3.2 ASTROMETRY OF GLOBULAR CLUSTERS AND DWARF SPHEROIDAL GALAXIES 14
3.2.1 Outstanding Questions *14*
3.2.2 Astrometry with MICADO *14*
3.2.3 Globular Clusters *15*
3.2.4 Dwarf spheroidal galaxies *16*
3.2.5 Instrument Requirements *17*
3.3 RESOLVED STELLAR POPULATIONS UP TO VIRGO 17
3.3.1 Outstanding Questions *17*
3.3.2 Extending the study of resolved stellar populations up to Virgo *18*
3.3.3 Galaxies in Virgo: Late types *20*
3.3.4 Galaxies in Virgo: Early Types *22*
3.3.5 SFH from the Horizontal Branch *23*
3.3.6 Instrument Requirements *24*
3.4 RESOLVED STRUCTURE AND PHYSICAL PROPERTIES OF HIGH REDSHIFT GALAXIES 24
3.4.1 Outstanding Questions *24*
3.4.2 The need for MICADO at E-ELT and science goals for high z studies *25*
3.4.3 Imaging high redshift galaxies: structure and colours *25*
3.4.4 Imaging high redshift galaxies: emission line mapping *28*
3.4.5 Instrument Requirements *28*
3.4.6 Impact with respect to other similar facilities *31*
3.5 FORMATION AND EVOLUTION OF GALACTIC NUCLEI AND BLACK HOLES 31
3.5.1 Outstanding Questions *31*
3.5.2 The central structure and supermassive black holes in nearby galaxies *32*
3.5.3 QSO Host Galaxies *35*
3.5.4 QSO Environments *39*
3.5.5 Instrument Requirements *40*

4 MICADO IMAGE SIMULATOR **41**

4.1 MAGNITUDE LIMITS FOR ISOLATED POINT SOURCES 43
4.2 EXAMPLE 1: A SIMULATED CROWDED FIELD 46
4.3 MAGNITUDE LIMITS FOR GLAO 48

5 SCIENCE TRADE-OFF **50**

5.1 MICADO OPTIONAL MODES 50
5.1.1 Coronagraphy *50*
5.1.2 Ground Layer Adaptive Optics *51*
5.1.3 A Grism Spectroscopic Capability on MICADO *54*

5.1.4 Polarimetry 59
5.1.5 Simultaneous Colour Imaging 59
5.1.6 Tunable Filter 60
5.1.7 High Time Resolution Astronomy 61

6 APPENDIX: SCIENCE TRADE-OFF TABLE 62

ABBREVIATIONS AND ACRONYMS

AO	adaptive optics
CAD	computer aided design
CAE	computer aided engineering
ECSS	European Cooperation for Space Standardization
E-ELT	European Extremely Large Telescope
ESO	European Southern Observatory
FDR	Final Design Review
FTE	Full Time Equivalent (year)
GLAO	ground layer adaptive optics
GMT	Giant Magellan Telescope
JWST	James Web Space Telescope
LESIA	Laboratoire d'Etudes Spatiales et Instrumentations pour l'Astrophysique
LTAO	laser tomography adaptive optics
MAIT	Manufacture, Assembly, Integration, Test
MAORY	Multi-conjugate Adaptive Optics Relay
MCAO	multi-conjugate adaptive optics
MICADO	Multi-adaptive optics Imaging Camera for Deep Observations
MPE	Max-Planck-Institut für extraterrestrische Physik
MPIA	Max-Planck-Institut für Astronomie
NOVA	Nederlandse Onderzoekschool voor Astronomie
OAPD	Osservatorio Astronomico di Padova
PAE	Preliminary Acceptance in Europe
PAO	Preliminary Acceptance at the Observatory
PA/QA	Product Assurance / Quality Assurance
PDR	Preliminary Design Review
PSF	Point Spread Function
RTD	Real Time Display
SCAO	single-conjugate adaptive optics
TMT	Thirty Meter Telescope
USM	Universitäts-Sternwarte München
WP	Workpackage

CONTRIBUTING AUTHORS

L.R. Bedin, R. Bender, E. Cappellaro, R. Falomo, N.M. Förster Schreiber, M. Franx, R. Genzel, L. Greggio, E. Held, K. Jahnke, K. Kuijken, A. Milone, E. Noyola, T. Paumard, G. Piotto, A. Renzini, H.-W. Rix, R. Saglia, A. Shearer, E. Tolstoy

1 SCOPE

This document describes the set of science cases and science trade-offs developed for MICADO as part of the Phase A Study. These have been used to drive the specifications and hence the design of the instrument.

2 APPLICABLE AND REFERENCE DOCUMENTS

2.1 Applicable Documents

The following applicable documents form a part of the present document to the extent specified herein. In the event of conflict between applicable documents and the content of the present document, the present document shall be taken as superseding.

AD1 Common definitions and acronyms , E-ESO-SPE-313-0066, Issue 1

AD2 E-ELT Interfaces for Scientific Instruments, E-TRE-ESO-586-0252, issue 1

AD3 Call for Proposal For a Phase A Study of a High Angular Resolution Camera for the E-ELT, Specifications of the Instrument to be studied, E-ESO-SPE-561-0097, v2.0

AD4 Statement of Work for the Phase A Design of MICADO, E-SOW-ESO-561-0127, v1.0

2.2 Reference Documents

RD1 Standard Procedure for Design Reviews, VLT-INS-ESO-00000-0251, issue 2

RD2 Guideline for Review of PDR Data Packages, VLT-INS-ESO-00000-0313, issue 1

RD3 Science Case and Requirements for the ESO ELT- Report of the ELT Science WG, dated 30.4.2006

RD4 Proposal “MICADO: the MCAO Imaging Camera for Deep Observations”, 12 Nov 2007, in response to the call CFP/ESO/07/17768/LCO

RD5 High Precision Astrometry with MICADO at the E-ELT, Trippe et al., MNRAS submitted

RD6 MICADO System Overview, E-TRE-MCD-561-0009, v2.0

3 SCIENCE CASES

In this Section a description is given of what the consortium considers to be the most important and most interesting science issues that MICADO will allow one to attack. The main requirements for MICADO resulting from each science case are reported in the attached Trade-Off Table. In doing so the consortium has taken notice of the initial science cases put forward by the E-ELT SWG. Unlike the SWG science cases, the present science cases are related to a specific instrument, the performance of which has been set by the Technical Specifications attached to the ESO call for proposals, as listed in the document E-ESO-SPE-561-0097 (AD3). As such, these science cases offer an exploration of the concrete limits that can be achieved in imaging with the E-ELT.

As an imager, MICADO will have a combination of angular resolution, field of view, and near-IR sensitivity that will be unsurpassed by any other imager on the ground or in space. As a long-slit spectrograph, it will also offer for some years an unsurpassed combination of angular and spectral resolution and sensitivity. These capabilities open to MICADO many opportunities for breaking new ground in several areas of cosmology and astrophysics. For this Phase A study we have developed into detailed "Science Cases" a relatively small number of such opportunities that we consider to be the most important, in order to distill from them a set of requirements to drive the design of the instrument.

The performance of MICADO makes it the ideal instrument to study the nuclei of galaxies, closer to their centres than ever done so far. This applies first to the Galactic Centre itself, with the possibility of mapping stellar orbits and flaring gas closer and closer to the event horizon. Then, in relatively nearby galaxies MICADO will make it possible to measure the mass of central black holes with great accuracy, as well as to check for the presence of multiple black holes, central disks and star clusters, and study their dynamics. Finally, MICADO will offer the possibility of resolving at high redshift the quasar light from that of the host galaxy, tracing the evolution with redshift of the black hole mass vs bulge mass relation, shed light on the mechanism of AGN feedback, as well as on the role of environment in triggering AGN activity.

The superior angular resolution of MICADO makes its astrometric applications especially attractive, and every effort should be made to ensure the short and long term stability of the instrument. Besides mapping stellar orbits near the central black hole in the Galaxy, astrometry of globular cluster stars should allow astronomers to measure trigonometric parallaxes and proper motions of these stellar systems with unprecedented accuracy, as well as reveal whether they harbour intermediate mass black holes near their centres. Similarly, astrometry of stars in dwarf spheroidals, coupled to their radial velocities, will permit to map the dark matter distribution within these smallest galaxies, possibly setting constraints even on the physical nature of dark matter particles.

Galaxy formation and evolution remains a central theme in observational cosmology, and with MICADO it will be possible to gather unique information both on local as well as high redshift galaxies. For example, studies of star formation histories from stellar colour-magnitude diagrams could be pushed well within the main body of galaxies all the way to the distance of

Virgo. On distant, high redshift galaxies the multi-wavelength broad-band and narrow-band imaging will reveal many details about the structure and physical processes in galaxies at the epoch of their peak star formation activity, mass assembly, and morphological transformations.

The MICADO consortium has also investigated the potential of a possible wide field option of the instrument, with the AO module working in GLAO mode. To this end, a science case on a survey for high redshift supernovae has been developed. It shows that such a version of MICADO (although in reality this would actually have to be a completely different instrument in itself) would not be competitive with other supernova searches, from either the ground or from space. Thus, the Consortium does not deem worth studying further a possible GLAO/wide field instrument. Instead, for supernova science the long-slit mode of MICADO would offer a powerful tool for measuring redshifts and types of the most distant supernovae discovered by other deep surveys.

3.1 The Galactic Centre

3.1.1 Outstanding Questions

The Centre of the Milky Way is a unique laboratory for exploring strong gravity around the closest massive black hole (MBH), and for studying fundamental and broadly relevant processes happening in a very dense star cluster surrounding this MBH, at a level of detail and quality that will not ever be possible in external galaxies (Figure 1). The Galactic Centre also serves as a crucial guide for theoretical studies of accretion onto MBHs and the important issue of co-evolution of MBH activity and nuclear star formation.

Arguably the most fundamental goal of Galactic Centre research in the next decade(s) will be dynamical measurements of the gravitational potential ever close(r) to the event horizon, with the ultimate goal of testing General Relativity in the strong field limit. The currently available observations with the VLT and Keck of the orbits of ~ 30 bright 'S-stars' in the stellar cusp around the MBH coincident with the compact radio source SgrA* provide the best tool available in astrophysics today for clean dynamical measurements of the gravitational potential to a scale of $\geq 10^3$ times the radius of the event horizon, R_s (left panel of Figure 1). For comparison, the best observations in external galaxies sample $>3\times10^4$ R_s. The VLT/Keck observations are strongly limited by confusion. Fainter stars than presently observable are very likely present, as the observed K-band luminosity function (KLF) is very steep (Figure 2). In addition, the volume density of the S-stars increases inward with $R^{-1.3\pm0.1}$, such that there is a very good chance that higher resolution measurements will find fainter stars at 10^2-10^3 R_s. At that radius, orbital velocities approach 0.1c and orbital periods may be as short as a few years, allowing the detection of the effects of Special and General Relativity (SR and GR) on these orbits. Such measurements will test SR and GR in a hitherto completely unexplored regime of field curvature and mass scale (right panel of Figure 1). Still further in, at a radius of a few R_s, variable infrared emission from transiently accelerated electrons ('flares') probe the innermost accretion zone around the MBH. Detection of orbital motions of this hot gas requires an astrometric precision of about 10 micro-arcseconds on time scales of a few hours.

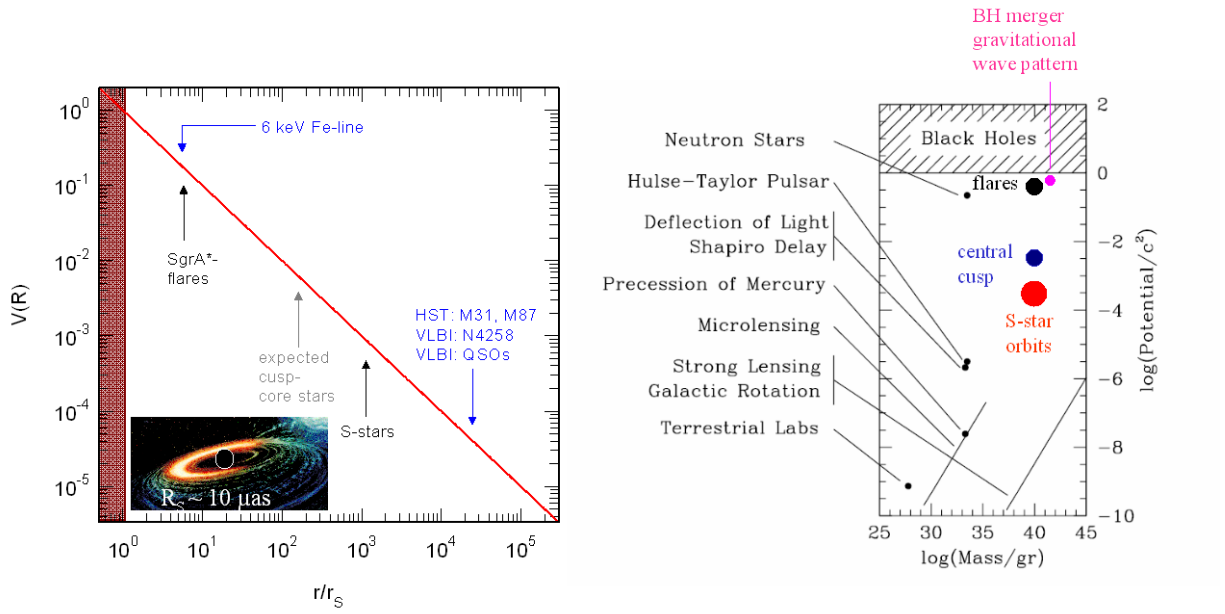

Figure 1: left: Gravitational Potential around a (massive) black hole, as a function of radius in units of the radius of the event horizon. Current dynamical measurements in the Galactic Center ('S-stars') probe to ~1000 R_s, while external galaxies (blue) probe to ~3x10^4 R_s. Measurements with MICADO/EELT will probe faint cusp stars ten times further to the event horizon, where β^2-effects of Special and General Relativity, as well as the Schwarzschild precession term can be observed. GRAVITY-VLTI observations of infrared flares and potentially also spectrally resolved X-ray reverberation mapping of the 6.4 keV Fe-line may be able to push dynamical measurements into the very strong curvature regime at a few times R_s. Right: comparison of different probes of gravity, as a function of mass scale (horizontal) and field curvature (vertical). The Galactic Center stellar orbits and flares probe a hitherto totally untested regime of mass and field curvature.

Because of the effects of confusion mentioned above, the current precision of astrometric measurements is significantly worse than the fundamental measurement limit. Higher resolution observations (with higher precision and lower confusion) are required for detecting the Newtonian precession of these orbits due to any extended mass outside of the central MBH. Such a distributed mass distribution consists of the observed stars themselves ($<10^2$ $M_\odot$ in the central 0.1") and in addition, stellar remnants (stellar BHs and neutron stars: estimated to be $\leq 10^4$ $M_\odot$) and perhaps dark matter. Detection of these components is obviously of great interest, especially also for determining the expected rates of extreme mass ratio in-spiral events leading to gravitational waves.

Another important issue is whether gas falling into the nuclear region forms stars near the MBH, or whether it is accreted directly into the hole, and whether nuclear star formation and MBH activity are related. Current observations of the Galactic Centre have yielded the remarkable result that episodic star formation deep in the sphere of influence of the MBH appears to be efficient, and apparently has a top-heavy mass function. A better quantitative

determination of the processes involved in stellar formation in this extreme environment, a precise determination of the resulting stellar mass function and the exploration of the connection between the rates of star formation and black hole accretion are critical for understanding the cosmological co-evolution of galaxies and MBHs.

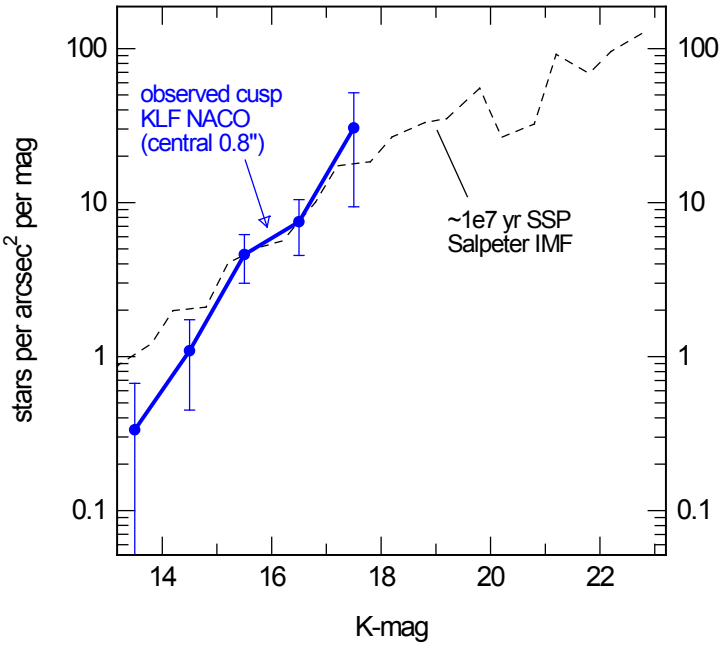

Figure 2: Observed K-band luminosity function (KLF) of the central 0.8", as observed with NACO on the VLT (blue), compared to a t=10^7 yr age population with a Salpeter IMF (dotted black). Combined with the observed $R^{-1.3+/-0.1}$ power law, stellar density distribution, this means that there likely are 5-10 K<20 stars in the central 0.1-0.2".

Finally the Galactic Centre MBH (SgrA*) is the prototype of the very common class of highly radiatively inefficient accretion sources (L/L_{edd}~$10^{-8....-6}$). Detailed multi-wavelength observations of SgrA* are beginning to shed light on the complex physics underlying this inefficient accretion process that appears to dominate at relatively low accretion rates and is guiding current theoretical work. Future work will emphasize high time resolution, spectrally resolved observations and polarization studies. Astrometry of the 'infrared' flares will be extremely exciting but probably requires ~10μarcsecond resolution.

3.1.2 Science drivers and capabilities of MICADO at the EELT

MICADO & EELT are uniquely suited for the exploration of a number of the above key issues in the Galactic Centre. The central stellar cusp around SgrA* is strongly confusion limited for current AO observations on 8m class telescopes, limiting the reliable detection and measurement of position of stars to K~16-17.5, which corresponds to main sequence B-stars. The combination of MICADO and the EELT will push the effective stellar detection sensitivity

by ≥5 magnitudes in modest integration times, making studies of even sub-solar mass stars possible and allowing mass function studies across the entire range of stellar masses. Extrapolating from our current work in the Galactic Centre and from the astrometry study that is part of this program (RD5) it will be possible with MICADO to carry out astrometry at a long term precision of 50-100 μarcsec, 3 to 6 times better than currently with NACO at the VLT. At that level of precision a number of key issues of the physics of massive black holes and their surroundings can be tackled. MICADO research on the Galactic Centre will likely concentrate on the following issues:

- detection of β^2 (β=v/c) post-Netwonian effects of SR and GR, as well as possibly the Schwarzschild pro-grade precession term, for some of the orbits of the already known S-stars to K~17.5, in particular the stars S2 and S14, which have the smallest peri-bothroi (15-20 light hours). Because of the confusion with fainter stars these effects will almost certainly not be measurable in proper motion data with current 8m-class telescopes, even with great patience;
- detection of the theoretically predicted cusp of stellar remnants (stellar black holes and neutron stars) by the Newtonian retro-grade precession of the apo-bothroi of the known S-stars. Of special interest is the possible detection of more massive intermediate mass black holes that have been hypothesized to form in dense star clusters outside the Galactic Centre and then secularly sink into the central cusp by dynamical friction. The determination of this dark cusp is of great general importance for predicting event rates for LISA large mass ratio in-spiral events. Simulations show that MICADO will be able to determine the mass of this extended dark halo around the MBH with an accuracy of less than a few percent (Figure 3);
- determination of the orbits of fainter (K≤20-21) main sequence stars in the inner cusp, with semi-major axes significantly smaller than the current S-stars, using both astrometric data and Doppler spectroscopy. Extrapolations from the surface density distribution and KLF indicate ~5-10 stars with K≤20 (m≥1.4 M_{sun}) in the innermost 0.1-0.2", of which a few stars may have peri-bothroi $<10^3$ R_s, several times smaller than that of S2. Such stars would have orbital time scales of a few years. In this case the Schwarzschild precession term and other GR terms will be detectable in a decade of observations (Figure 4).
- study of the central accretion zone surrounding SgrA*. With the resolution of the EELT (5-10 mas) it will possible to study in detail the spectral and temporal properties of accretion events and search for evidence of outflows/jets predicted for radiatively inefficient accretion flows as in the Galactic Centre. Short term astrometry within an accretion event, as well as the search for positional shifts between accretion events at different times are of great interest for finding evidence for orbital motion and outflow of the hot gas and the predicted Brownian motion of the central massive black hole;
- with the outstanding astrometric precision of the EELT (50-100μarcsec) it will be possible to determine orbits of $\sim 10^{2.5\text{-}3}$ individual stars over a decade of observation. From such data it will then be feasible to determine the distance to the Galactic Centre to 0.1-0.3%, thus enabling a number of powerful constraints on the dynamics of the Galaxy (Figure 3). It will also be possible to explore stellar phase space clumping directly (such

as the one or two disks of young massive stars already known), binary fractions and to search for possible intermediate mass black holes in the central cluster;

- outside of the central parsec, EELT astrometry will allow dynamical measurements of the other prominent young star clusters in the central 50 pc (Arches, Quintuplet etc.). Perhaps the most intriguing issue is the search for possible intermediate mass black holes there (as in globular clusters). The unambiguous detection of an intermediate mass black hole in such a cluster has far-reaching consequences for seed black hole formation during the epoch of reionization;
- with the high angular resolution and enormous sensitivity of the EELT & MICADO it will be possible to count stars to <1 M_{sun} and establish the present day mass function. In combination with colors and spectra it will then be possible to determine a robust initial mass function in the Galactic Centre and test the emerging evidence that the IMF in the Galactic Centre region is much flatter than that in the Galactic disk.

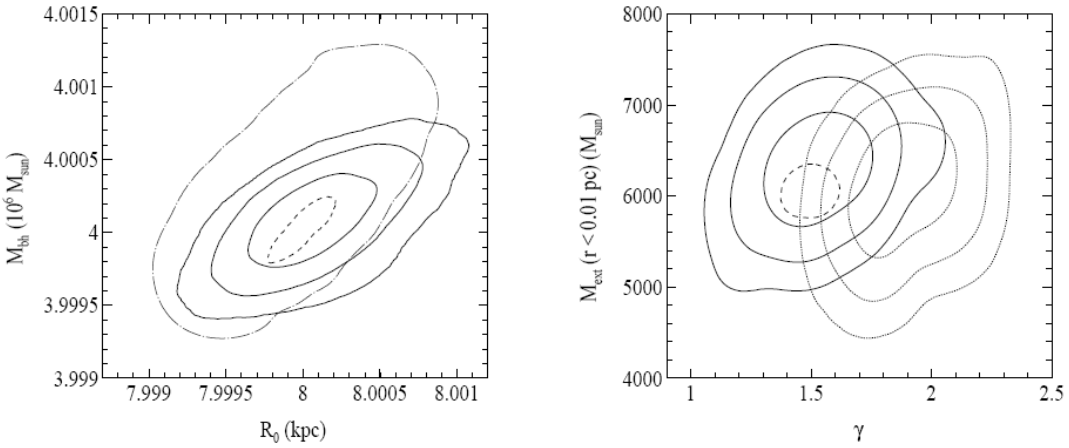

Figure 3: Examples of the precision of parameter estimations in the Galactic Center, obtained from simulations of stellar orbital astrometric and radial velocity data with an ELT (taken from the TMT study by Weinberg, Milosavljevic & Ghez 2005), Left: 1, 2 and 3σ uncertainty contours (solid) of mass and distance to the Galactic Center MBH obtained from an astrometric study of 20 stars with a modest precision of 500μarcsec and 10 km/s. The dotted contour gives the 3σ contour for a 5 times higher precision, which will be achievable with MICADO. Right: Same for the estimate of the extended mass around the MBH for two different choices of the power law slope γ of the cusp's density distribution.

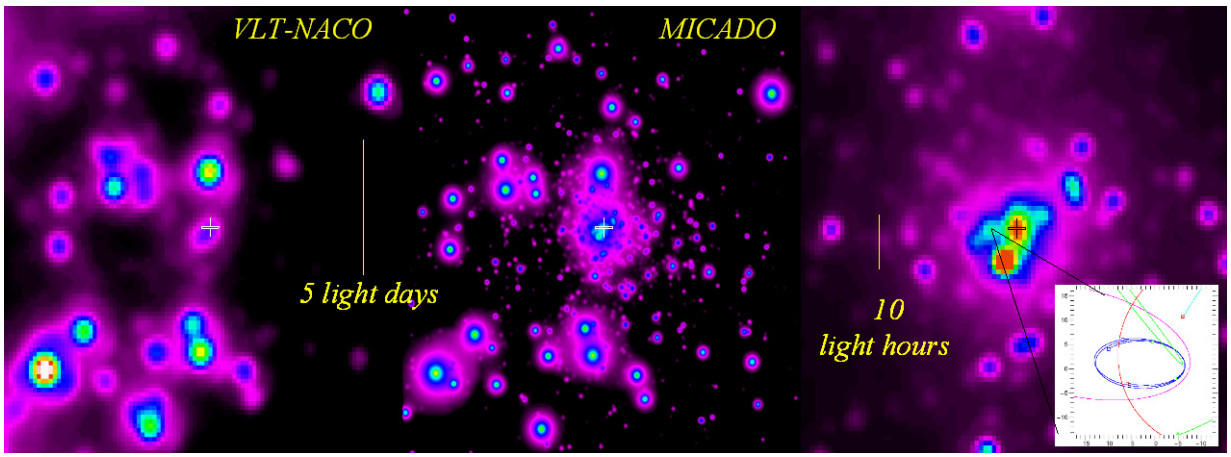

Figure 4: How will MICADO images of the central cusp around the MBH look? The left panel shows a current high-quality VLT/NACO K-image at 60 mas resolution. Using the KLF- and surface density information obtained from these data and extrapolating to fainter magnitudes with a Salpeter IMF (Figure 2) yields the simulated MICADO image in the central panel (on the same scale as the NACO image), also applying the current best model of the PSF. The right panel then shows a zoom into the central region of this image. A number of stars in this image are close enough to the central MBH (cross) that the Schwarzschild precession of their orbits may be observable for sufficiently high ellipticity, as depicted in the simulation in the lower right.

3.1.3 Instrument Requirements

It is obvious from the discussion above that the most important instrument requirement for Galactic Centre research is high quality (50-100μarcsec), stable (time scale of years) astrometry and a stable, diffraction limited (Strehl ratio >30%) PSF. Our astrometric study shows that achieving the astrometric goals in the highly crowded central stellar cusp around SgrA* requires substantial oversampling of the PSF, with a desired pixel scale of 1-2 mas. The required photometric accuracy is ~0.05 to 0.07 mag. Other important requirements include a high throughput, near-diffraction limit spectroscopic capability (for measuring radial velocities from faint star spectra), and a moderately large field (10-20”). A polarization capability is desirable for studying the time evolution of the highly polarized ‘flare’ events in the immediate vicinity of the event horizon of the MBH. Simultaneous wavelength coverage of several photometric bands for variability studies in these flares would also be useful. The Galactic Centre studies rely mostly on H and K band observations, perhaps with an option to extend to J band.

3.2 Astrometry of Globular Clusters and Dwarf Spheroidal Galaxies

3.2.1 Outstanding Questions

Globular clusters are the oldest known components of the Milky Way, and tracing their formation may reveal important aspects of the early formation of the Galaxy itself. Measuring parallax distances with MICADO, along with their proper motions will allow us to construct the 3D kinematics of a major fraction of the globular cluster system, and their orbits within the Galactic potential. This should allow us to address questions such as whether kinematic families exist among globular clusters, suggesting that they may have formed within precursor galaxies that merged, contributing to the build up of the Galactic spheroid. Measuring accurate density distributions and proper motions of faint stars near the centre of individual globular clusters should reveal whether intermediate mass black holes exist in (some of) these stellar systems, hence enriching the problematic of globular cluster dynamical evolution and black hole formation.

Measuring the dark matter content of dwarf spheroidal galaxies is an interesting test of structure formation models. The internal motions of dwarf spheroidal galaxies can reveal the gravitational fields in these systems, which allows one to estimate the amount and distribution of dark matter in these objects, and even possibly to set constraints on the physical nature of dark matter particles.

3.2.2 Astrometry with MICADO

MICADO should enable unprecedented diffraction-limited proper motion measurements. Present ground based experience shows that with appropriate software and with properly sampled images we can reach an astrometric precision <1% DL (diffraction limit) or seeing disk FWHM, e.g. 7mas, or 0.03 pixels at the WFI@2.2m, corresponding to ~0.75% FWHM (Anderson et al. 2006). With properly dithered images, we can reach ~1% DL @500nm with the under sampled ACS@HST camera. It has been shown that the AO assisted NACO@VLT can reach an astrometric precision of 200μas, i.e., ~0.50% DL @1.2μm.

The corresponding expected astrometric precision for MICADO is at the level where many systematics could enter, and we need to consider all of them. In the following, we will assume an astrometric precision on a single MICADO image of 50μas (RD5). However, we note that, if we are able to control the systematics very well, in principle this precision could scale with the sqrt(N), where N is the total number of images over which the astrometric precision is reached. Optimistically one then might even be able to achieve a precision (with multiple images) down to <10μas with a >30m ELT (Cameron et al. 2009, AJ, 137, 83).

Adopting the 50μas astrometric precision given in RD5 implies a proper motion precision of 10μas/yr in 5yrs (5μas/yr in 10 years). In principle, we can even think of a 30yr baseline by using HST archive images, which, in the best cases, should allow an astrometric precision down to ~100 μas, i.e., over 30 years, we should be able to reach a proper motion internal error of: 3-4μas, for faint stars in crowded environments. In this respect, MICADO could be perfectly complementary to GAIA for proper motion measurements of faint objects, and/or for

highly reddened or crowded environments, and a number of interesting science cases can be foreseen.

3.2.3 Globular Clusters

Accurate astrometry of globular clusters stars allows one to address several important aspects concerning their formation and evolution, as well as their use as tracers of Galaxy formation, including:

Decontamination of cluster samples

The simplest use of the proper motion is the extraction of pure cluster sequences, after removal of field objects with proper motions significantly different from the cluster stars. The most obvious application is for clusters embedded in the Galactic bulge or in the Magellanic Clouds. Note that it is not necessary to have a cluster with a systematic motion with respect to the field (which would make the job easier), but we can also take advantage of the fact that the internal velocity dispersion of the cluster stars (which can be used as a proper motion reference frame) is much smaller (a few km/s) than the velocity dispersion of the field.

Cluster parallaxes

For parallax measurements, we need to consider the following reference number: at 1kpc we have a parallax semi-displacement of 1.0mas. Accounting for multiple images, and most importantly, for the fact that we can measure the parallax of a large number of stars, we expect to measure parallaxes of star clusters and stellar agglomerates at least out to the distance LMC with errors significantly smaller than 10%, i.e. for all of the Galactic star clusters, in particular those heavily obscured or in a crowded environments, which are not measurable by GAIA. Distances accurate to better than10% are a pre-requisite for obtaining cluster ages to better than 20%.

Internal motion and rotation of cluster stars

With a typical internal velocity dispersion of 5km/s the proper motion dispersion is 100 μas/yr at 10kpc, hence one can measure an internal proper motion field with errors significantly less than 10% in a few years out to a few tens of kpc. The only limiting factor for internal tangential motion field and rotation is the number of measured stars.

Absolute Motions of GCs and dwarf galaxies

The Proper motion precision on a single high S/N point source in 5 years is 10 μas/yr, and possibly better if using HST archive data. At 10kpc, 50km/s corresponds to1000 μas/yr, i.e. one single absolute reference source would allow a 1% precision in the absolute proper motion measurement.

At 100kpc, 200km/s corresponds to 400 μas/yr, i.e. one single point like reference source would allow a 2.5% precision.

The problem may be the lack of absolute point sources (QSO) in a single MICADO frame. In that case we can use many faint high-redshift galaxies, in particular taking advantage of quasi-point like sources within each of them. In this case one would need to reach galaxies at very

faint magnitudes. Globular cluster astrometry using faint galaxies for the astrometric reference has been successfully achieved with HST (Kalirai et al. 2007). Thus, obtaining the full 3D motion of virtually all Galactic globular clusters appears to be feasible with MICADO@EELT.

Binaries in GC cores

With 50 μas resolution one can measure the wobble of all binary members with a dark companion (BH, NS, WD) with a mass > 0.5 M_{sun} and separation > 0.5AU in a cluster out to 10kpc. The numbers scale accordingly for more distant clusters. Binaries for which both components are visible are harder to measure, but feasible.

The same observations would allow one to study the proper motion of stars very close to the cluster center, and therefore explore the presence of IMBH for clusters well beyond 10kpc.

3.2.4 Dwarf spheroidal galaxies

Measuring the dark matter content of dwarf spheroidal galaxies is an interesting test of structure formation models. The internal motions of dwarf spheroidal galaxies can reveal the gravitational fields in these systems. MICADO enables such measurements via diffraction-limited proper motion measurements.

CDM simulations of gravitational collapse show that dark halos should be very clumpy, a consequence of the hierarchical merging that characterises CDM cosmology. On the assumption that these clumps (sub-halos) host the dwarf spheroidal satellites, the mass function of the satellites should be similar to the high end of the theoretical mass function of clumps seen in the simulations. It will be important to attempt to establish this relation observationally: if it does not hold, it would point to a significant modification of the CDM structure formation mechanism, for example, to the disruption of these halos by early star formation and mass loss.

Intense radial velocity campaigns of dwarf spheroidals have been carried out in order to measure their dynamical masses. Typically, velocity dispersions stay flat out to large radii, suggesting indeed that rather massive halos surround the satellites. However radial-velocity measurements are subject to the orbit anisotropy degeneracy: a deeper potential can be mimicked by a tangentially biased orbit distribution. Proper motions are the way to break this degeneracy by directly measuring the shape of the velocity ellipsoid (ratio of the radial and tangential velocity dispersions) of the stars. A recent compilation of results for 23 dwarf spheroidal galaxies (Strigari et al, Nature 2008, Aug 28) concludes that over 4 orders of magnitude in luminosity the total halo masses of dwarf spheroidals are rather uniform. However, this remarkable result is affected by the unknown orbit distribution, and the observations envisaged here are precisely the measurements that will settle the issue.

In the following feasibility calculation it is assumed that MICADO will be capable of measuring diffraction-limited positions over a full field. With careful PSF-matched astrometry, many dithers and a dense star field, it is possible to reach precisions in relative astrometry down to 1% of the PSF FWHM (this does require a total S/N of the order of 100 on each star, but sensitivity is not the limiting factor in this project). Such precision has been achieved with HST astrometry in the bulge and in crowded fields. For MICADO on a 42m E-ELT, at 1μm

wavelength, this corresponds to ~60 μas. Over a 5-year baseline this means that a12 μas/yr proper motion dispersion is measurable, corresponding to 5.5 km/s at a distance of 100kpc.

This accuracy is more than sufficient to measure the shape of the velocity ellipsoid in these systems, given internal radial velocity dispersions of around 10km/s. Much more dynamical information, such as the relaxation level of the systems, detailed distribution functions, behaviour at the tidal radius, etc., can be obtained by combining a proper motion survey with radial velocity measurements of the same stars. Note that the above only concerns relative astrometry. Absolute astrometry, which can be used to derive orbits of the satellites in the galactic potential, would be very interesting as well, but requires a proper reference frame. This could be established by identifying background QSOs or compact galaxies in the field. Such measurements could be performed with single-year baselines.

3.2.5 Instrument Requirements

The proposed applications assume an astrometric precision of 50 μas on a single well exposed image. Multiple images could improve the precision. A goal of 50 μas astrometric precision on single image should be our minimum target. For this, it is mandatory to control all the possible systematic effects, keeping to a minimum the geometric distortions, calibrating them away, and ensuring their stability over time baselines of many years. A quantification of the requirements on mechanical flexures needs to be developed, also with the help of appropriate simulations. Placing MICADO in a gravity invariant location is highly preferable, given the prominent role played by the astrometric applications of the instrument.

A 30 arcsec field of view appears to be adequate for most applications, although a wider field of view would help recovering the necessary absolute reference objects (AGN and faint distant galaxies), and to properly map the internal kinematics of dwarf spheroidals, which extend over many arcminutes.

3.3 Resolved stellar populations up to Virgo

3.3.1 Outstanding Questions

One of the key issues in modern astronomy concerns the Star Formation History (SFH) in the universe. Indeed, while the development of structures is well understood in terms of hierarchical growth in the framework of the Cold Dark Matter (CDM) model, it is still not clear how to couple the baryonic component to the CDM. Direct observations of galaxies up to high redshift can be used to map the SFH, but since the integrated galaxy light is dominated by the most recent stellar generations, the information on the underlying older stellar population is severely limited. A similar problem affects the analysis of the spectral energy distribution of galaxies, from which only luminosity averaged ages and metallicities can be derived. The SFH in galaxies can be uncovered by interpreting the Colour-Magnitude Diagrams (CMD) of their stars, the fossil record of the SFH. The key issues are therefore the following: what is the SFH

and metallicity distribution of galaxies as derived from the CMD of their resolved stellar populations? And how do they compare to the corresponding quantities as derived from integrated-light studies? Are such derived SFHs consistent with the evidence from observations of their likely precursors at high redshifts?

3.3.2 Extending the study of resolved stellar populations up to Virgo

With current instrumentation this type of study is feasible only in the Local Group and a little beyond: this implies a very limited sampling of the SFH in the universe, with plenty of dwarfs, a small number of spirals and almost no giant elliptical. Due to its large collecting area, the E-ELT will allow us to probe a wider volume, where we can access a more significant sample of galaxies. More importantly, because of crowding, stellar photometry in external galaxies is currently feasible only in regions of relatively low surface brightness. For giant galaxies, this prevents us from deriving detailed SFH where most of the galaxy mass is. The excellent resolution capabilities of MICADO will enable us to study high surface brightness regions, i.e. the inner parts of galaxies, where SF was more conspicuous, as well as to address directly age and metallicity gradients.

The decoding of the CMD in terms of SFH is based on the analysis of the stellar density distribution across the CMD, and relies on specific features of stellar evolution (e.g. Greggio 2002, ASP Conf. Ser. 274, 444). While stellar age-dating is most effective at the Main Sequence Turn-off (MS TO), some information on the SFH can be gained from Helium burning, Horizontal Branch (HB) stars, and also from the intrinsically brightest regions of the CMD. Actually, old stellar populations, with very faint TO, can be sampled at much brighter magnitudes at the end of their evolution on the Red Giant Branch (RGB). Figure 5 shows that old MS TO in galaxies beyond the Local Group are prohibitively faint even for MICADO @ E-ELT, while accurate photometry of bright RGB stars will be feasible up to the Virgo Cluster. RGB stars are also much less numerous than TO stars; therefore they can be effectively used as mass tracers in high surface brightness regions, where crowding prevents photometry of fainter stars. Figure 6 shows how in this respect MICADO@E-ELT is much more efficient than JWST. In the following, three applications are considered in more detail: a young and an old stellar population in Virgo, and the study of the HB stars in NGC3379, a nearby Elliptical Galaxy (DM=30.3).

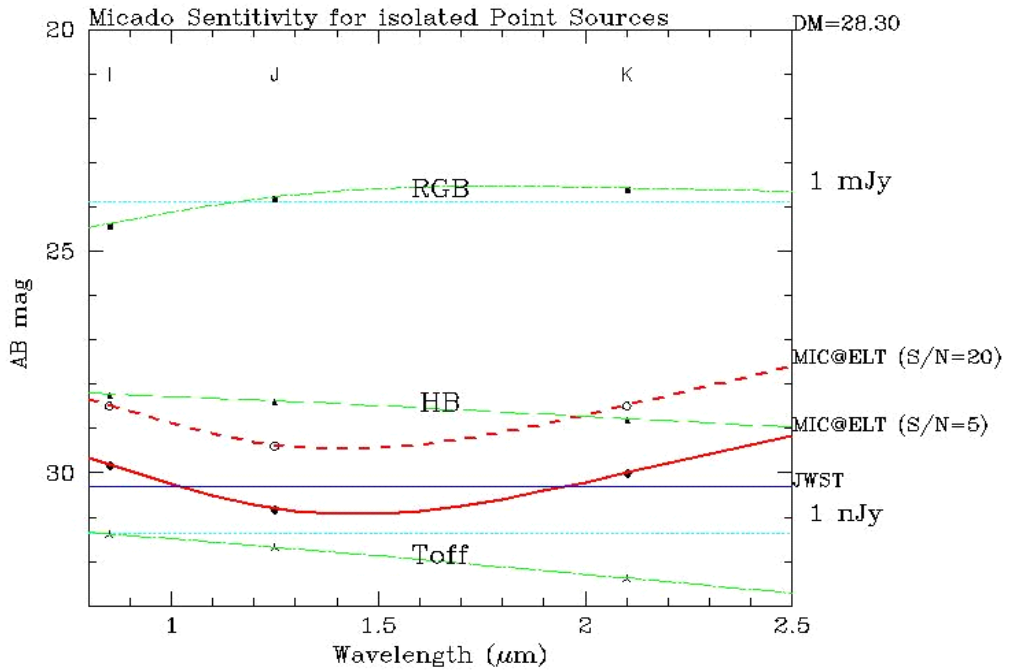

Figure 5: Limiting magnitudes as function of wavelength for isolated stars at DM=28.3 with a 5hr exposure, at different S/N ratio. The green lines show typical magnitudes of stars at the RGB tip, HB and TO for a solar metallicity 10 Gyr old stellar population. The JWST 5σ limit under the same conditions is shown as a blue line. While the sensitivity is comparable for isolated point sources, MICADO has a huge gain in resolution, as demonstrated in Figure 6.

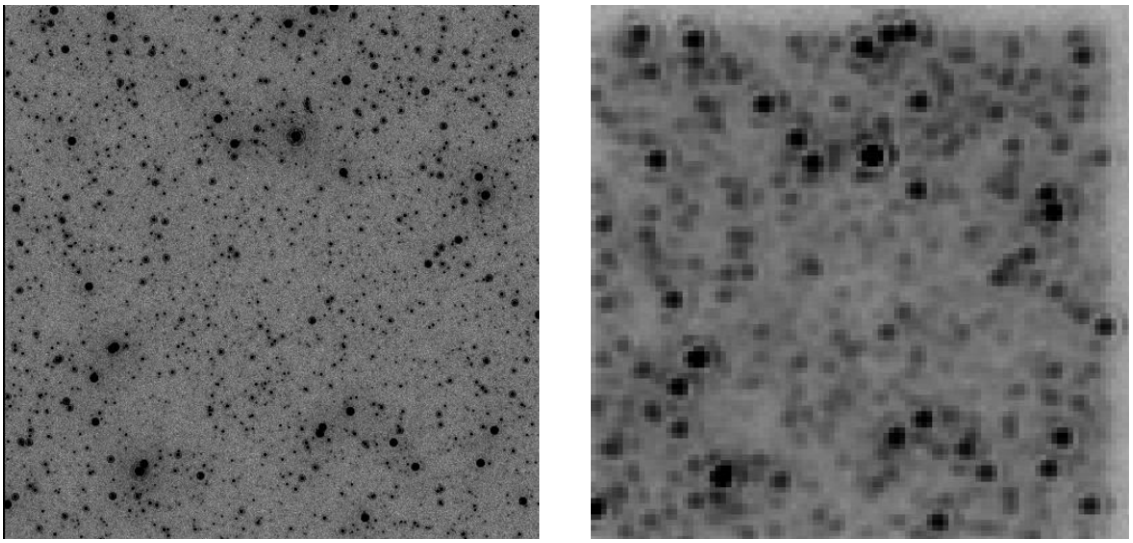

Figure 6: Comparison of a 5-hr K-band exposure of a simulated stellar field, observed with MICADO (left) and JWST (right). For MICADO, PSFs provided by ESO were used. The field was created using the simulator described in Section 4.

3.3.3 Galaxies in Virgo: Late types

The left panel of Figure 7 shows a synthetic CMD constructed with the ZVAR code (Bertelli, priv. comm.) with an input SFH appropriate for star forming galaxies. The four superimposed boxes target specific age ranges, and the number of stars in each box is proportional to the stellar mass formed within the relative age range. The age partition is illustrated in the right panel of Figure 7: the RSG box samples stars younger than 50 Myr; the BSG box stars from 50 to 100 Myr old; the AGB box collects stars from 100 Myr to 1.5 Gyr old; and the RGB box is populated with stars older than about 2 Gyr. The specific production of stars in each box (number per unit mass, or luminosity), function of the age and metallicity distribution of the stellar population, can be computed from stellar evolution, and used to sketch the SFH in a galaxy from simple star counts in the diagnostic boxes. For each box Table 1 lists the interesting parameters for this application. The third column shows that the statistics are large, so that the different age ranges are adequately sampled. An important issue in this kind of study is crowding, which can severely degrade the photometric accuracy: the fourth column shows that these SFH tracers are sparse enough even at a surface brightness (B-band) of 22mag/arcsec^2. Notice that the K band luminosity sampled by one resolution element is ~110L_{Ko}, safely below the faintest limit of the faintest box (~ 800 L_{Ko}). Accurate photometry of these bright stars will thus be feasible down to the very centers of the spiral disks. A more rigorous evaluation of the effect of crowding on the photometry, based on simulated images, is described in Section 4.

Table 1: Feasibility of the SFH study for galaxies at DM=31, hosting a composite stellar population as in Fig. 2, having assumed a FoV of 30" x 30", a pixel scale of 3mas, and a 10pixel resolution element. For each box (col.1) the other columns list: the specific production of stars (col.2), the number of stars sampled at a B surface brightness of 22 mag/arcsec^2 (col.3), the number of stars of each kind per resolution element (col.4).

BOX	$N_{STARS}/L_B\ (L_{B\,o})^{-1}$	N_{STARS}	N_{STARS}/N_{RE}
RSG	$7\ 10^{-7}$	388	$4\ 10^{-5}$
BSG	$3.5\ 10^{-6}$	1920	$2\ 10^{-4}$
AGB	$2\ 10^{-6}$	1080	$1\ 10^{-4}$
RGB	$1.3\ 10^{-4}$	70750	$7\ 10^{-3}$

Using different colour combinations, and/or a more precise description of the (rather uncertain) bright AGB phase we may improve on the age resolution for stars older than ~1 Gyr. Figure 8 shows selected isochrones in the (I, I-K) CMD, which appear to separate well in luminosity during the late stages of the AGB evolution. If observationally confirmed, this feature could be used to draw diagnostic boxes with an age resolution of 1-3 Gyr.

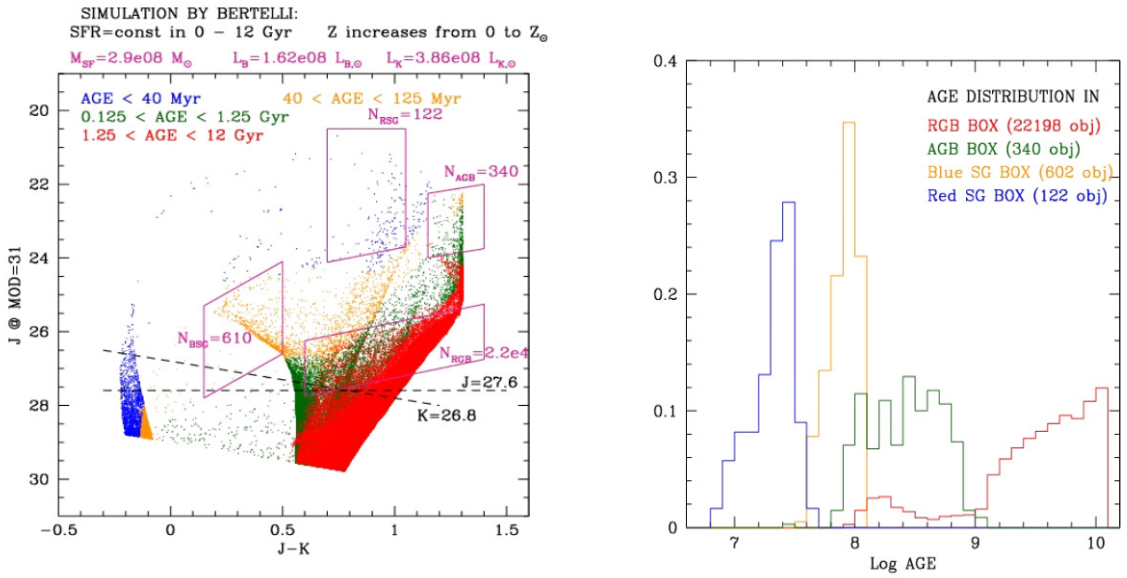

Figure 7: A synthetic CMD (left panel) for a stellar population constructed as specified in the upper label, with a Salpeter IMF between 0.1 and 100 Mo. The four diagnostics boxes considered in this exercise are superimposed; the age distributions of their sampled stars are shown in the right panel. The dashed lines in the left panel show the limiting magnitude for isolated stars with a 5 hr integration at S/N=10.

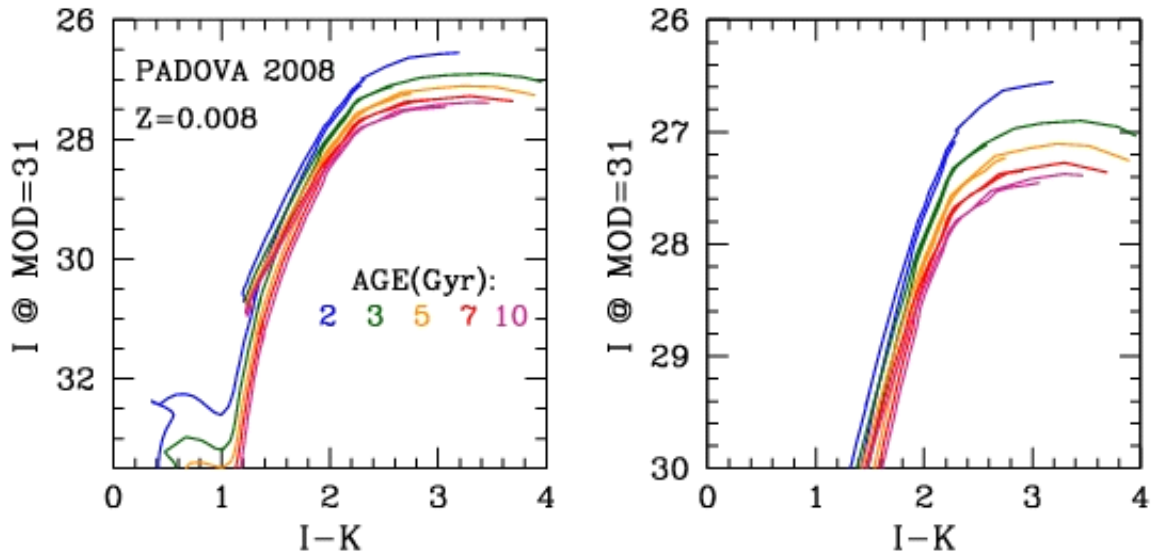

Figure 8: Isochrones from the Padova set which incorporate a detailed description of the thermally pulsing AGB phase (Marigo and Girardi 2007, A&A 469,239).

3.3.4 Galaxies in Virgo: Early Types

The CMD of old stellar populations shows the lack of stars in the RSG, BSG and AGB boxes, while the RGB box is populated proportionally to the total stellar mass sampled. In this case, a very important application of MICADO concerns the possibility of deriving the metallicity distribution in regions of high surface brightness, where current instrumentation cannot resolve individual stars. Due to the age-metallicity degeneracy, (i.e. metal poor, old stars have the same colors as metal rich, young stars) the mapping of the colour distribution into a metallicity distribution of RGB stars is not very precise; still, the colors of these stars are much more sensitive to metallicity than to age, so that a first order estimate of the metallicity distribution can be obtained from photometry (Harris, W.E. & Harris,G.L.H. 2002, AJ 123, 3108). Figure 9 shows a synthetic CMD for an old stellar population, with a wide metallicity distribution in 3 colour combinations: the different metallicity bins appear separated in colour, better in the (I-K) than in the (J-K) CMD, due to the higher temperature sensitivity of the wider colour baseline. This implies that one can obtain the same accuracy on the metallicity distribution tolerating larger photometric errors when using the (I-K) rather than (J-K) colour. On the other hand, a too wide colour baseline selects against high metallicity (reddest) stars. For the particular metallicity distribution explored, the detection in the I-band appears barely sufficient to include the most metal rich stars, while a similar detection threshold in the R band would imply a severe undersampling of the high metallicity tail of the distribution.

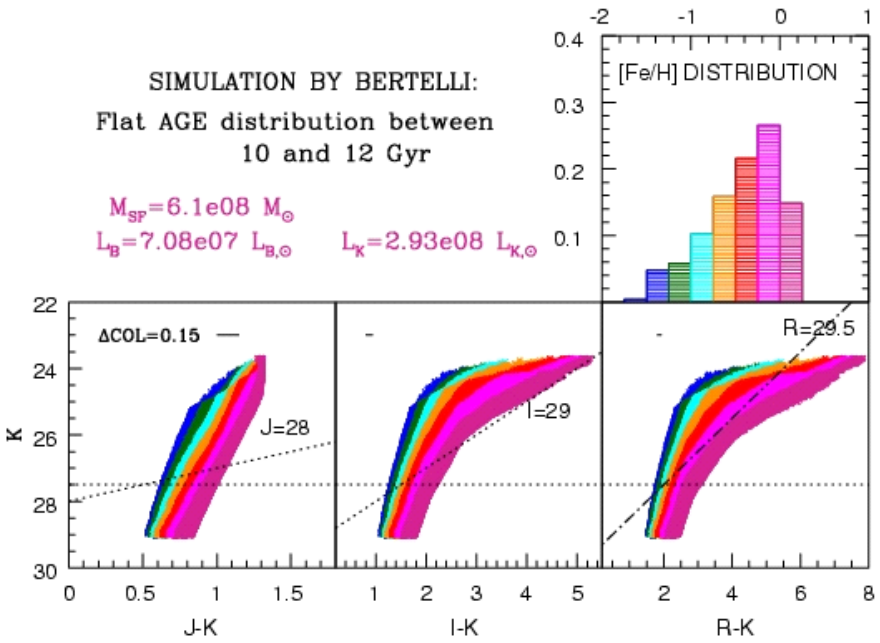

Figure 9: Synthetic CMD, for an old stellar population, at a distance modulus of 31 mag, with the metallicity distribution measured in Cen A (see Rejkuba et al. 2005), shown in the upper right panel. The parameters of the simulation, computed with the ZVAR code, are labeled. The colors encode the metallicity bin, and the dotted lines show the magnitude limits at S/N ~ 10 (for isolated stars) with ~5 hrs exposures.

The simulation in Figure 9 counts 1.24 10^{-4} stars per unit mass brighter than K=27.5, and its mass to light ratios are 8.33 and 2.1 respectively in the B- and K-bands (solar units). It follows that, for a distance modulus of 31, a FoV of 30" x 30" located at a surface brightness of 26.4 in the B band, collects 10000 stars, ensuring high statistics even at low surface brightness. Crowding conditions can be gauged by inspection of Figure 10. At a B surface brightness of 21 the number of stars per resolution elements is less than 0.1 over the whole magnitude range of interest (~ 2 upper magnitudes on the RGB) in both I and K. It should then be possible to derive the metallicity distribution in a typical elliptical well inside its effective radius.

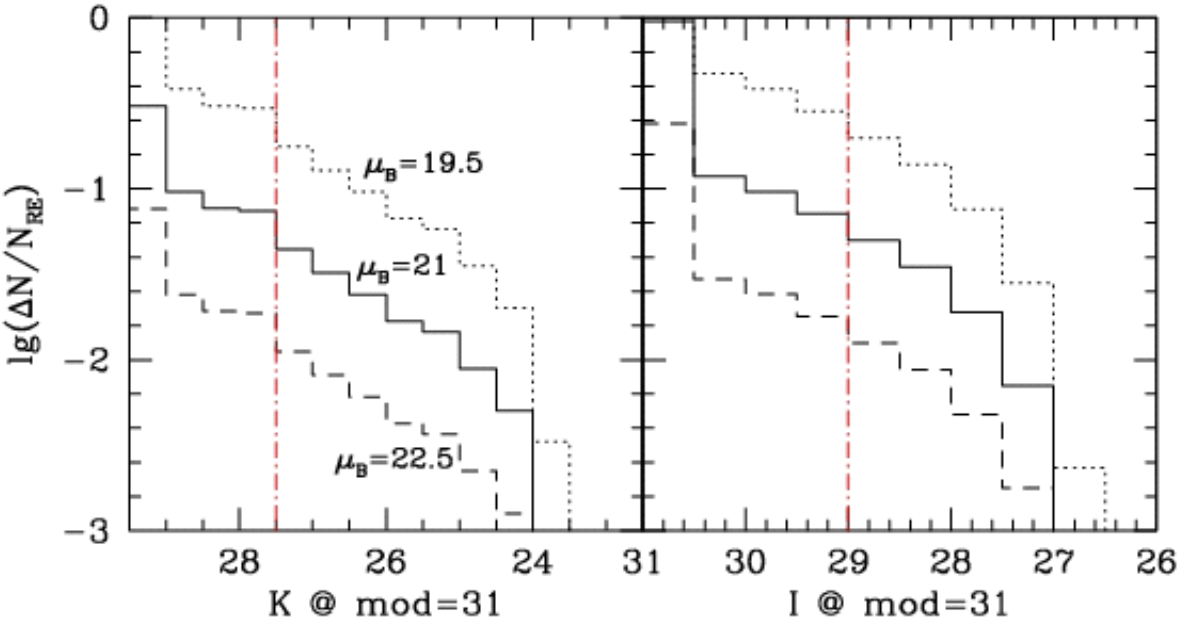

Figure 10: Number of stars per resolution elements as a function of the K (left) and I (right) magnitudes for the stellar population in Fig. 4, for 3 values of the B surface brightness, as labeled. A pixel scale of 3 mas and a resolution element of 10 pixels have been adopted. The red lines show the limiting magnitudes reported in Figure 9.

3.3.5 SFH from the Horizontal Branch

The stars' distribution on the HB can be effectively used to infer the SFH in galaxies. Noticeable features include the secondary clump (Girardi, L. et al. 1998, MNRAS 301, 149) which traces SF at ages around 1 Gyr, RR Lyraes and Blue HB stars, distinctive of truly old stellar populations. In order to derive the SFH from the core Helium burning stars in stellar populations older than ~2 Gyr an accurate analysis of the colour distribution is mandatory, which is best achieved with the synthetic CMD method (e.g. Tolstoy & Saha 1996), incorporating a careful description of the photometric errors.

NGC3379 (M105) is a Giant Elliptical Galaxy in the Leo Group. At a distance modulus $(m-M)_0$ ~ 30.3 its HB stars should be measurable at S/N~5 with 5 hrs integration (see Figure 5). The specific production of HB stars is ~500 every 10^5 solar luminosities in the B-band of the

parent stellar population. Therefore, at a surface brightness of 23.2 in the B band, there are ~0.05 HB stars per resolution element. This can be considered as an upper limit for reliable photometry, since the RGB + AGB component of the stellar population counts almost as many stars as the HB (at magnitudes brighter than the HB itself). For M105, the surface brightness at the half-light radius (r_e = 28.5arcsec) is $I(R_e)$ = 15.5 mag/arcsec^2 in K (16.5 in J). Since for a typical elliptical B-K ~ 4, the study of the HB population in M105 will be feasible only in the outer parts at such large distance.

From the analysis of these three Science cases we conclude that MICADO@E-ELT will enable us to derive the SFH in galaxies as far as the Virgo cluster, and to do this in regions of high surface brightness, including most of the galactic stellar mass. Figure 5 shows that the sensitivity of JWST is comparable to that of MICADO; however, given the pixel scale of 30 mas, crowding effects are ~ 100 times worse. This implies that MICADO will allow us to study the stellar populations in nearly the same cosmological volume as JWST, but at a surface brightness brighter by as much as ~5 mag. This unique capability is very important to effectively investigate the SFH across the main body of giant galaxies, rather than just in their outskirts.

3.3.6 Instrument Requirements

A FoV of 30”x30” with a pixel scale of 3 mas seems adequate for the study of the SFH in galaxies up to Virgo. A smaller pixel scale (1-2 mas) may allow us to reach areas of somewhat higher surface brightness, an aspect being currently investigated with simulations. SFHs can be derived reliably using only near-IR bands, but the I-band is necessary to investigate the metallicity distributions as well as to derive the SFH from the HB population. A photometric accuracy of a few 0.01 magnitudes is sufficient for the above science cases, a large Strehl ratio, and a well mapped PSF are required to ensure the required photometric quality over the whole frame.

3.4 Resolved structure and physical properties of high redshift galaxies

3.4.1 Outstanding Questions

What do high redshift galaxies look like? Do they show signs of (secular) instabilities and bulge build up? Are there AGN lurking in their centres? What are the physical processes driving the evolution of galaxies towards their present appearances?

Imaging and integral field spectroscopy at the VLT and imaging with HST of high redshift (z ~ 2) galaxies with ~ 1 kpc resolution have revealed that galaxies of all morphological types differ radically from local, low redshift galaxies. Disks have much higher gas velocity dispersions, gas mass fractions, and star formation rates than their local counterparts, and ellipticals appear to be much smaller and denser for a given stellar mass. With its wider aperture and better sampling, the E-ELT+MICADO will achieve a factor 5 to 10 improvement in resolution

compared to the VLT (and HST), hence providing multi-colour images of high redshift galaxies with a richness of detail approaching that currently possible only for relatively nearby galaxies. This quantum jump in resolution and sensitivity will allow us to map the star formation rates, stellar ages, and dust distributions in very distant galaxies on scales of ~100 pc or better, distinguish the bulge components and measure their sizes and ages, look for the presence of AGN, search and characterize populations of young massive (super) star clusters, etc. This will enable us to pinpoint the physical processes that are shaping galaxies at the epoch when mass build up and morphological differentiation are at their peak.

3.4.2 The need for MICADO at E-ELT and science goals for high z studies

The physical processes driving galaxy formation and evolution are still an enigma. Given the most recent results from high resolution studies (imaging and integral field spectroscopy, from the ground and from space) it is now becoming clear that galaxies at redshift $z \sim 1 - 4$, when they were undergoing their most rapid phase of stellar mass assembly, were very different from local galaxies. High redshift galaxies have higher rates of gas accretion and star formation, and more intense radiative and mechanical feedback from star formation and AGN. Most $z > 1$ star-forming galaxies look irregular and very often clumpy in current imaging (e.g., Conselice et al. 2004; Elmegreen et al. 2004, 2007, 2008; Law et al. 2007a). Kinematic mapping indicates they are far more gas-rich and turbulent than $z \sim 0$ galaxies, implying they are unstable and should fragment into self-gravitating units (e.g., Förster Schreiber et al. 2006; Genzel et al. 2006, 2008; Tacconi et al. 2006, 2008; Erb et al. 2006; Law et al. 2007b). Despite these new insights, the detailed workings remain elusive. Theoretical models and numerical simulations still do not reproduce satisfactorily the observed characteristics of individual galaxies and of galaxy populations, at high redshift and consistently across cosmic epochs to the present day. This is largely attributed to simplified and often inadequate recipes for the complex phenomena that govern the evolution of galaxies such as feedback, merger and mass accretion history, redistribution of mass and angular momentum, chemical enrichment, heating/cooling processes, etc. The main limitation is spatial resolution: at best, resolutions of $\sim 50 - 100$ mas can be achieved with current telescopes, even with adaptive optics (AO). This corresponds to $\sim 400 - 800$ pc at $z \sim 1 - 4$, and provides a limited number of resolution elements across typical high redshift galaxies. This is clearly insufficient to resolve substructure on scales of individual giant star-forming complexes and clusters, which is necessary to pin down the physical and dynamical processes involved. This is where MICADO at the E-ELT will provide new and unique observational constraints and will allow the next major leap forward in understanding the early evolution of galaxies.

3.4.3 Imaging high redshift galaxies: structure and colours

High resolution imaging of $z > 1$ galaxies will thus be crucial for a proper understanding. Their typical sizes are $\sim 0.2 - 0.3$ arcsec at $z \sim 2 - 4$, decreasing at higher redshift roughly as $1/(1+z)$ at fixed rest-frame luminosity (e.g., Bouwens et al 2004), and decreasing with lower luminosity (roughly as $L^{0.5}$). High resolution imaging with HST generally gives very few resolution elements, at a level of 10 within an effective radius. This is equivalent to imaging Virgo

galaxies with10 arcsec seeing! Moreover, it has also become clear that quiescent galaxies at high redshift tend to be very small and dense – they are still unresolved with HST (e.g., Toft et al. 2007; van Dokkum et al. 2008; Cimatti et al. 2008). The E-ELT will provide a unique capability to image these galaxies. The presence of substructure on <~ 100 pc scales in high redshift galaxies is not a trivial issue, but some studies suggest it is very likely: near-IR integral field spectroscopy of a few strongly lensed z ~ 1 – 3 galaxies shows clumps on physical scales of ~ 100 pc (Swinbank et al. 2006); imaging of local analogs of z ~ 3 "Lyman-break galaxies" contain super star clusters (Overzier et al. 2008); and numerical simulations of turbulent gas-rich disks show that the Jeans-scale kpc-sized clumps may further break up into smaller-scale structure (F. Bournaud, priv. comm.).

Hence it is clear that the high resolution imaging capability afforded by a diffraction-limited camera such as MICADO on the E-ELT will provide direct insight into the dynamical state of the galaxies and into the processes that drive their evolution. More specifically, observations at the diffraction limit (6,8,10 milliarcsec in J, H, K) will correspond to approximately 60 pc in physical length (for z > 1), and will be of comparable quality to 1 arcsec imaging of VIRGO galaxies. This will allow us to isolate and even resolve regions with sizes comparable to individual star-forming complexes such as 30 Dor in the LMC, N66 in the SMC, or super-star clusters seen in nearby starburst galaxies. Furthermore, this resolution will typically provide >100 resolution elements across the galaxies, and deliver detailed information about the morphology, dynamical state, and variations in stellar/physical parameters across the galaxy (see Figure 11 and Figure 12).

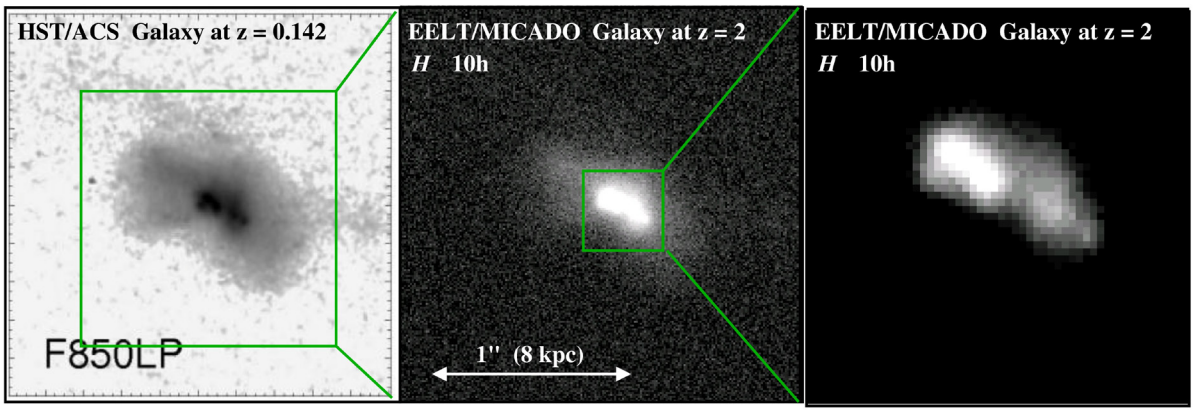

Figure 11: Simulation of MICADO observations of a high redshift galaxy. An ACS image of a z=0.142 galaxy by Overzier et al. (2008; left panel) has been transposed to z=2 (middle panel). The surface brightness is typical of high surface brightness galaxies at z~2. The simulated observation is taken in the H band and corresponds to a 10 hour integration with MICADO. The middle panel has a field of view of 2″ × 2″, and the right panel zooms in on the center. The inner structure of the galaxy is clearly visible. MICADO at the E-ELT will provide unprecedented resolution allowing us to investigate the detailed structure of high redshift galaxies on physical scales as small as 60–100 pc.

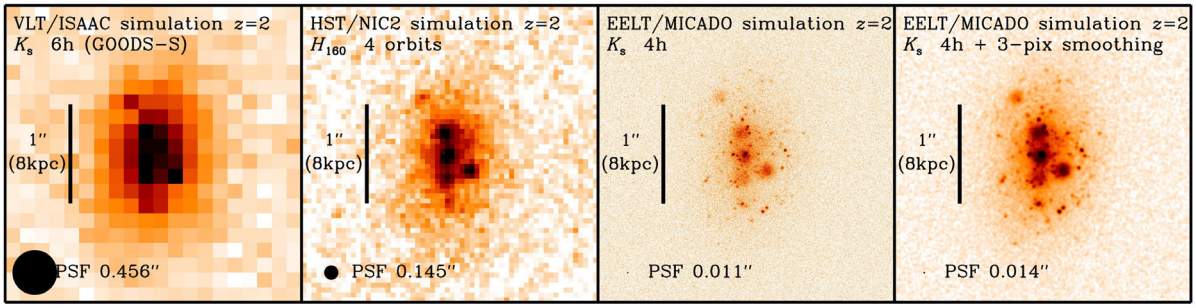

Figure 12: Illustration of the gain in resolution with MICADO at E-ELT. From left to right, the panels show a simulated z=2 galaxy in deep but seeing-limited ground-based observations (6 hours with VLT/ISAAC in K, equivalent to data of the GOODS-South field), deep diffraction-limited HST/NICMOS observations (4 orbits with NIC2 camera in H), and similar integration time of 4 hours with E-ELT/MICADO in K, at a resolution of about 10 mas or 80 pc at z=2 (about 10 times better than with HST/NIC2). The mock galaxy has been created so as to resemble a real bright and large galaxy (K_{AB} ~ 21.3 mag, half-light radius ~ 5 kpc) with very prominent clumpy structure that was observed with HST/NIC2 (Förster Schreiber et al., in prep.), including a smooth underlying component and several kpc-sized clumps. In addition, a few hundred compact (unresolved) clusters were added with a range of magnitudes. The clumps and clusters contribute roughly 40% of the total light of this simulated galaxy. Compact clusters to K_{AB} ~ 28.5 mag are well detected. A small amount of smoothing (with a Gaussian of FWHM equal to that of the PSF) enhances the rich structure one might be able to detect with such MICADO observations. A key goal that we will be able to achieve with E-ELT/MICADO is to resolve the kpc-size substructure observed in many high redshift systems, but which is at the resolution limit of current instrumentation.

Two aspects are considered in this high-redshift science case: high resolution imaging for spatially-resolved structure and colours and emission line mapping. The latter is highly desirable with narrow-band imaging over the full field of view and, as a further possibility, through a tunable filter device (such as a Fabry-Perot) as part of the additional arm with smaller pixels and field of view (discussed separately below). Both share similar science goals.

Key science goals include:

1) ***Galaxy structural parameters***: light profiles and effective radii of compact/dense quiescent galaxies, nascent bulges and disks; disk/bulge growth; structure and properties of merger progenitors; internal structure: secular evolution versus external processes, redistribution of mass and angular momentum (presence and characteristics of bars, density waves, tidal features in mergers and from clumps interactions), star formation triggering mechanisms; morphology- vs colour-density relations, etc.
2) ***Clump structural parameters***: light profiles and effective radii of large-scale (kpc-scale) clumps, investigate whether clumps resolve into substructure ("super star clusters"), mass profiles to test whether intermediate-mass black holes can be formed in clumps (later coalescing at the galaxy's nucleus).

3) ***AGN and host galaxy properties***: supermassive black hole growth, galaxy/AGN co-evolution, feedback processes; nuclear fuelling processes.

4) ***Distribution of dust and stellar age***: obscuring dust geometry, mode of star formation ("cluster" vs "distributed" modes, as in local starburst galaxies), properties of kpc-sized clumps (super star clusters and giant HII regions; their sizes, masses, stellar populations, star formation rates, metallicities, dust content, etc.).

5) ***Spatially-resolved star formation histories***: star formation timescales on "local", i.e., < 100 pc scales, and on galaxy-wide scales as reconstructed from the spatially-resolved star formation history within galaxies; stellar mass build-up of different structural components, chemical evolution, etc.

6) ***Super Star Clusters***: Search for putative luminous/massive star clusters; if such exist and are detected, characterize their spatial distribution across the host galaxies (confined to kpc-sized clumps or more widely distributed?), as well as their age distribution and luminosity/mass function in order to test scenarios for their formation, constrain processes dominating the dynamical evolution of super star cluster populations, establish whether they are linked to the halo, spheroid, and thick-disk components of present-day galaxies, and investigate if they are the progenitors of globular cluster systems in local galaxies.

3.4.4 Imaging high redshift galaxies: emission line mapping

Extremely valuable information about galaxies can be gained from line emission, which map out HII regions, shock-excited interstellar medium (ISM), and outflows from star formation and/or AGN. For $z \sim 1 - 4$, lines of Hα, Hβ, [NII], [OIII], [OII], [NeIII] become accessible in the near-IR, which provide diagnostics of the star formation rate, extinction, excitation sources, gas-phase abundances, densities, and ionization parameter. Ideally, the aim is to obtain spatially-resolved mapping in this entire set of lines. Very few redshift slices allow one to obtain all those lines simultaneously within telluric windows and between the night sky lines (roughly about 5 redshifts for filter width corresponding to $R \sim 200 - 300$: $z \sim 2.175$, 2.24, 2.295, 2.34, 2.395). For a filter wheel holding 20 filters, one could cover 3 – 4 redshift ranges.

An attractive add-on to MICADO in this context is a tunable interferometric device such as a Fabry-Perot (+ order-sorting filters), affording far more flexibility in terms of the combination of lines and redshift slices that could be explored. This would be implemented within the additional arm and thus foreseen for a smaller field of view of ~ 8 sq. arcsec.

3.4.5 Instrument Requirements

To achieve the above high redshift science goals, the following technical considerations have highest priority:

S/N estimates: S/N calculations indicate that integration times of 10 hours should be sufficient to study galaxies at z~2. This will give S/N > 10 for galaxies with moderate to high surface

brightness. However, galaxies with lower intrinsic surface brightness, or galaxies at higher redshift, will require longer integration times.

The full potential of diffraction-limited cameras such as MICADO at the E-ELT is realized for point-source sensitivity, i.e. studying resolved substructure. Recent work on nearby Lyman-break analogs has shown that they contain super star clusters (Overzier et al 2008), the kind of structure that will become accessible with MICADO/E-ELT. Their typical absolute magnitudes are of order of −17 AB mag at rest-frame optical wavelengths, corresponding to apparent ~ 27.8 AB mag at z ~ 2 or a range of ~26.3 – 29.0 for z ~ 1 – 4. These can therefore be detected directly with MICADO in 1 – 4 hours with S/N ~ 10. In 10 hours, we can reach 1 mag fainter, and thus investigate the presence of even lower luminosity substructure.

Field of view and pixel scale: Overall, a key objective is to study at least ~ 1000 galaxies to cover the known diversity of morphologies at high z, and allow investigations as a function of redshift and mass. This requirement is more important than actual pixel scale for the options under study (2 – 4 mas/pixel). With a typical density of 5 sources per sq. arcmin at K(Vega) < 21 mag, this implies an area of 200 sq. arcmin, comparable to 1 GOODS-sized field. With a field-of-view of 1 sq. arcmin and fiducial 10 hr integrations, this will take 2000 hours. It is therefore clear that a large field-of-view is essential, to allow building up a sufficiently large sample.

For emission line mapping with narrow-band filters of "redshift spikes", the field size needs to be sufficiently large to encompass proto-clusters. The earliest and most massive protoclusters found to date (around radio galaxies) at z ~ 2 – 5 are ~ 1.5 – 2 Mpc across, translating into 3 – 4 arcmin (e.g., Venemans et al. 2007). Less massive structures may be smaller. Hence, the (large) field size requirement is important for this science case. Observing more than a few galaxies at a time requires the full field of MICADO, hence multiple narrow-band imaging would be possible only for the multiple narrow band filter option.

For the Fabry-Perot option, the small field of view makes it relevant only for single-object or perhaps compact groups / multiple mergers, as 8 arcsec corresponds to ~ 70 kpc at z ~ 1 – 4. This would nevertheless provide extremely valuable and unique mapping of line emission, tracing e.g. giant complexes of HII regions with much more flexibility than with a fixed set of narrow-band filters.

PSF: The PSF needs to be well described over the full field, so that consistent and accurate photometry can be done over all galaxies observed. Good characterization of the PSF is essential to derive accurate structural parameters and colours (and line ratios, line-to-continuum ratios). Experience indicates that for these purposes, PSF characterization to < 10% accuracy is needed (encircled energy and FWHM being the critical parameters here). Acceptable variations across the field of view are of < 5%. A further consideration motivating these requirements is that typical observing strategies for deep imaging of high redshift galaxies involve many exposures dithered within boxes ~ 10 arcsec on a side, meaning the effective PSF at any location is complex and an average over all co-added frames, so too large variations over this scale of ~ 10 arcsec will result in significant loss of effective resolution.

Therefore, a PSF reference is essential for this science case and ideally would be constructed from stars in the observed field. However, the stellar density is low in any typical high-redshift

"deep field". We will therefore need an "external" characterization (e.g., from MAORY). Furthermore, we need high PSF uniformity, fidelity, and stability (spatially and temporally), and likewise for the distortion pattern, given the dithering strategy. Given a smooth 2D PSF model, deviations in shape should not exceed a few % across the field.

Photometry: For colours (and line and line-to-continuum ratios), relative photometric accuracy needs to be ≤ 0.03 mag (for comparisons with e.g., evolutionary synthesis model predictions and the ability to distinguish gradients in stellar parameters such as age, extinction, metallicity).

Wavelength coverage: For sufficient diagnostic power to reliably distinguish age, extinction, and metallicity, one needs a sufficiently long wavelength baseline. Ideally, one would like to bracket the age-sensitive 4000Å/Balmer break. For $z \geq 2$, this is achieved with $\lambda = 0.9 - 2.2$ μm (rest-frame range $\geq 3000 - 7300$ Å).

Observing strategy — dithering: This is a requirement on the telescope side. For accurate flat fielding and background subtraction, one needs to observe with many dithered frames. For broad-band imaging, the typical integration per dithered position is of order of the time variability of night sky lines, ~ 1 – 2 minutes (assuming no OH suppression is available). The typical dither box size is ~ 10 arcsec on a side (accounting for typical surface density of galaxies in any given field at all redshifts and typical galaxy sizes). For narrow-band imaging or the Fabry-Perot option, integration times can be factors of several longer than for broad-band imaging between night sky lines, so dithering would be less frequent.

Simultaneous colours: It would be desirable to have the capability for simultaneous "colours", for imaging with broad- and narrow-band filters. While image quality will be wavelength-dependent, simultaneous colours will likely minimize the time-dependence of PSF variations. The motivation is to increase photometric and PSF-matching accuracy.

Width of narrow-band filters: For emission line mapping with narrow-band filters, we set the requirement on filter band pass considering that the most massive protoclusters known at z~2-5 have typical velocity dispersions of ~ 500 – 1000 km/s (Venemans et al. 2007). Hence, R ~ 300 – 500 would ensure mapping of protocluster members across the full MICADO field of view. With this, the maximum shift of central wavelength across the currently planned ~ 45 sq. arcsec field should be $<\sim$ 500 km/s, or $\Delta\lambda <\sim 0.002 - 0.004$ μm (J to K band) or < 0.2%. Increasing the filter width relaxes this requirement to some extent, but also implies possible contamination by telluric night lines (unless an OH suppression device is implemented).

For the Fabry-Perot option, a typical high-redshift galaxy would have an integrated line width or velocity gradient of up to ~ 100 – 200 km/s, implying in this case $R >\sim 500$ is desirable (and up to ~ 2000), with again the maximum shift of central wavelength across the 8 sq. arcsec field required to be < 0.2%. Taking a Fabry-Perot as example, typical finesse is 30 – 50, and for a FWHM ~ 500 km/s (R ~ 500), ~ 7% order-sorting filters would be needed (a few per J, H, K band).

Throughput: Clearly for studying faint distant galaxies, throughput should be maximized. For a Fabry-Perot, the overall efficiency could be enhanced by tilting the etalon, splitting the continuum and emission line in the beam and thus obtaining a simultaneous measurement.

3.4.6 Impact with respect to other similar facilities

MICADO at the E-ELT will surpass JWST performance in angular resolution, by a factor of about 6; studies of individual high redshift galaxies on scales of < 100 pc will simply not be possible with JWST.

Compared to near-IR diffraction-limited cameras planned or under study for other ground-based 30 – 40 m class telescopes (Giant Magellan Telescope GMT; Thirty Meter Telescope TMT), MICADO will be highly superior in the field of view it will provide (~ 45 – 50 arcsec across compared to ~15 arcsec for others). For imaging high redshift fields, this will then provide a unique and substantial "multiplexing" advantage.

References

Bouwens, R. J., et al. 2004, ApJ, 611, L1
Cimatti, A., et al. 2008, A&A, 482, 21
Conselice, C. J., et al. 2004, ApJ, 600, L139
Elmegreen, D. M., Elmegreen, B. G., & Hirst, A. C. 2004, ApJ, 604, L21
Elmegreen, D. M., et al. 2007, ApJ, 658, 763
Elmegreen, B. G., Bournaud, F., & Elmegreen, D. M. 2008, ApJ, 688, 67
Erb, D. K., et al. 2006, ApJ, 646, 107
Förster Schreiber, N.M., et al. 2006, ApJ, 645, 1062
Genzel, R., et al. 2006, Nature, 442, 786
Genzel, R., et al. 2008, ApJ, 687, 59
Law, D. R., et al. 2007a, ApJ, 656, 1
Law, D. R., et al. 2007b, 669, 929
Overzier, R., et al. 2008, ApJ, 677, 370
Swinbank, A. M., et al. 2006, MNRAS, 368, 1631
Tacconi, L. J., et al. 2006, ApJ, 640, 228
Tacconi, L. J., et al. 2008, ApJ, 680, 246
Toft, S., et al. 2007, ApJ, 671, 285
van Dokkum, P. G., et al. 2008, ApJ, 677, L5
Venemans, B., et al. 2007, A&A, 461, 823

3.5 Formation and evolution of Galactic Nuclei and Black Holes

3.5.1 Outstanding Questions

Among the outstanding issues in galaxy evolution several concern galactic nuclei and their supermassive black holes: how they form and evolve, how their properties depend on the galaxies around them, and how they may affect the evolution of the host galaxy itself. These issues range from the formation of galaxy cores, central star clusters and supermassive black holes, to the mechanisms of mass transport into these central regions and the influence of the galaxy-scale and larger environment. A suite of different mechanisms is expected to be at work, spanning the nine orders of magnitude in linear scales from galaxy environments down to the

sphere of influence of a central black hole. Of even wider interest is the question as to whether QSO/AGN feedback is the physical process responsible for quenching star formation as massive star forming galaxies evolve into passive spheroids. In turn, what are the physical processes triggering nuclear activity? What is the role of environment (via interactions and/or merging)? MICADO has the potential to address all these questions thanks to a combination of diffraction limited resolution with high sensitivity and an adequately wide field of view.

3.5.2 The central structure and supermassive black holes in nearby galaxies

In the past decade, HST observations of local early-type galaxies have shown that two types of cores are present in these objects, correlated with absolute luminosity, kinematic anisotropy and isophote shapes of the galaxy. While early-type galaxies brighter than MB ~ -21 have well resolved so-called cuspy cores, fainter ellipticals and bulges have power-law centres that, at the distance of Virgo and with the optical resolution of HST, appear unresolved (Lauer et al. 2007). Supermassive black holes have been detected in these galaxies, which are expected to have a (destructive) influence on their surroundings (Merritt et al. 2007). Therefore, higher resolution imaging is expected to resolve the power-law cores and measure their core radii. MICADO at the ELT will be able to achieve 0.01 arcsec resolution in the K band with optimal AO and thus detect core radii down to approximately one pc at the distance of Virgo. Sensitivity is not an issue, since the increase in collecting area with respect to HST will more than compensate the factor 100 decreased size of the resolution element.

Using MICADO to image the nuclei of galaxies closer than Virgo will allow the possible detection of rings and disks similar to the ones seen in the Milky Way and M31 (Bender et al. 2005; 2009) and also extremely compact bar-type structures like the one found in NGC 3706. For example, the (blue) nuclear disk detected in M31 would be resolvable out to a distance of 7 Mpc (see Figure 13). The presence of eccentric nuclei will be detected at twice this distance or even in Virgo. Additional J or H band imaging will measure the associated colour gradients to constrain the stellar populations of the nuclear entities. At smaller distances, it should be possible to resolve single red supergiants that might be present in such circumnuclear disks. For example, assuming that Cen A is at a distance of 4.3 Mpc (or a distance modulus of 28.4) and that it has a central disk of blue stars similar to M31, it will be possible to resolve 5-10 supergiants in that disk (plus a background population of a few dozens old supergiants along the line-of-sight). The blue disk would have an area ~ 0.05 arcsec2 at this distance. Both old and young stars are bright enough (J=-3 to -5, J-H=1 for the former, 0.5 for the latter type) that their colours can be measured and used to distinguish the two populations. Assuming that the astrometric position of these red supergiants can be measured with a precision better than 1/3 of a pixel mas (for 3 mas pixels), or 0.02 pc in Cen A, one can detect the motion of a star moving at 2000 km/s over a period of 10 years.

Mergers of ellipticals and early-type spirals imply mergers of central black holes. While dynamical friction quickly leads to the formation of a compact black hole binary, the timescale over which this binary merges into a single black hole is highly uncertain. Hints for binary black holes have been found in a few cases at large distance only (e.g. OJ 287, Valtonen et al.

2008) but a systematic high resolution survey of nearby galaxy nuclei could produce highly interesting nearby candidates.

Finally, the resolution and light collecting power of an ELT may also allow one to detect flares in nearby galaxy nuclei that are similar to the ones observed in the Milky Way (Trippe et al. 2007). For these observations a polarimetry option could be interesting.

The Auxiliary Arm will allow imaging with smaller pixels (1.5mas) for a 6"x6" field of view. All the programs sketched above can profit from smaller pixels, enhancing the PSF sampling and possibly allowing better astrometric performances, and do not suffer from the smaller field of view. The larger scale (4 mas pixels) does not add to the scientific output

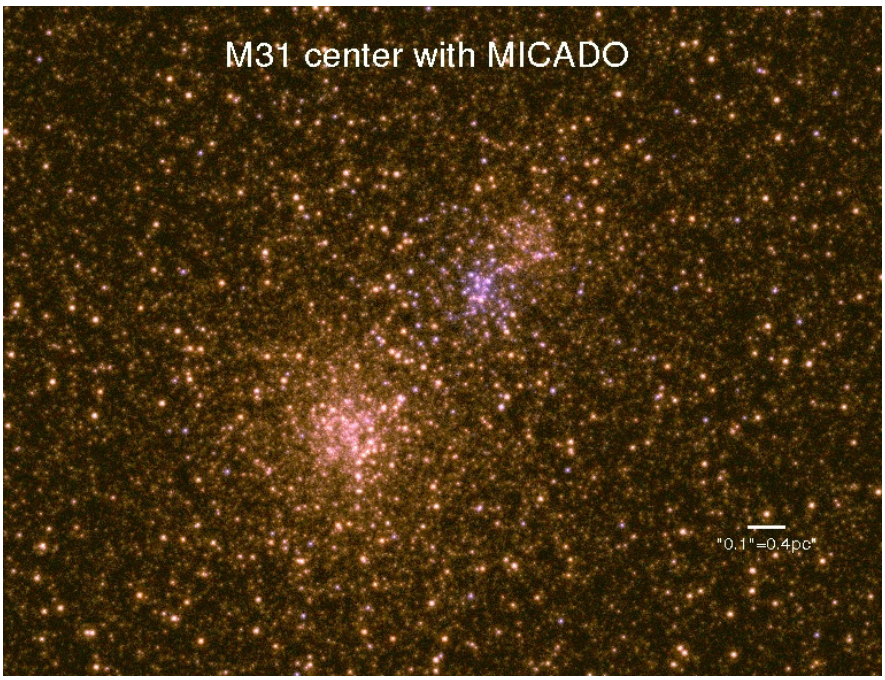

Figure 13: The core of M31 at the resolution of MICADO. Since the MAORY psf is still preliminary, we used an HST psf scaled to the MICADO resolution. The image has 3 mas size pixels and is ~2.5 arcsec on the side.

The availability of a long-slit grism spectroscopy mode through the 'Christmas Tree' would highly enhance the science output of MICADO. The determination of the radial velocities of resolved stars (up to the distance of Cen A) together with the astrometric data would allow the complete reconstruction of the orbits, similar to what has been done for the Galactic centre. Similarly, the radial velocities of resolved stars in Galactic globular clusters might allow the mass determination of intermediate mass black holes. Moreover, the stellar kinematics of the (unresolved) centres of galaxies could be measured. A spectral resolution of R~3000 for a 0.01 arcsec wide slit (σ_{instr}~40 km/s, ~15 km/s per pixel in the 1.5 mas pixel configuration) is needed to avoid the sky lines in the K band and resolve the typical velocity dispersions at the centres of (spiral or low-luminosity) galaxies. If a higher spectral resolution mode is available (R~5000), this would enable measuring velocity dispersions as low as 20 km/s. With this spectral resolution, Figure 14 shows the sphere of influence of a black hole of a given mass as a

function of angular distance, where we use the Tremaine et al. (2002) relation to link black hole mass to velocity dispersion, and we show galaxies with black hole mass determinations from stellar and gas kinematics. At the moment direct measurements are lacking at the low σ end, and are essentially limited to the nearest galaxies. MICADO will be able to spatially resolve the dynamical influence of "seed black holes" in local inactive bulge-less or dwarf galaxies (using the rest-frame CO band heads in the K-band out to ~50 Mpc) and the supermassive ones of inactive massive ellipticals out to redshift z~0.35 (using the rest-frame H-band). Assuming that sensitivities comparable to SINFONI will be achieved, the increase in collecting power of E-ELT compared to the VLT compensates ¼ of the flux reduction due to the increased resolution in case of constant surface brightness. Taking our SINFONI experience into account (Nowak et al. 2007) we expect to reach high-enough spectral signal-to-noise ratios to derive stellar kinematics with integration times on the order of 10 hours for local dwarf ellipticals or low-luminosity bulges. For the case of local bright ellipticals, where SINFONI observations require ~8 hours exposure time, several nights integrations would be needed to compensate for the distance of z~0.35 objects. Note that these science cases exploit the observed K band, where the maximum Strehl ratio is achieved. The availability of a larger spectral range at the same spectral resolution adds to the science results by increasing the effective spectral signal-to-noise ratio only if the achievable Strehl ratio (and therefore overall spatial resolution) at shorter wavelengths is above 20%. This will probably be true only for the H band, therefore, the present science cases would profit from H and K coverage, but not from further extensions to shorter wavelengths.

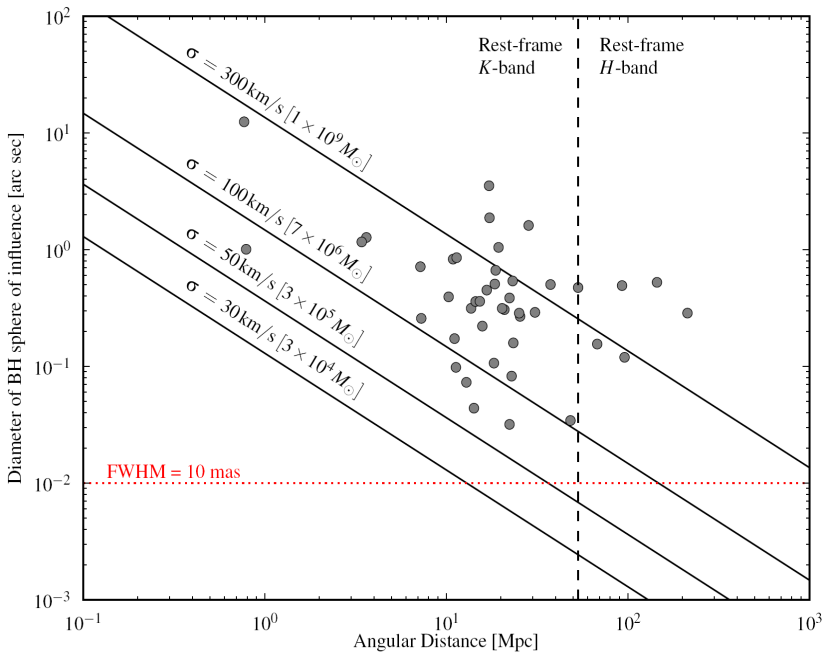

Figure 14: The size of the sphere of influence of a black hole as a function of its mass and distance. The red line shows the spatial resolution achievable with MICADO.

3.5.3 QSO Host Galaxies

Almost a decade ago it was discovered that not only all massive galaxies (should) contain a supermassive central black hole, but also that a quite tight relation exists between the mass of the black hole and the stellar mass of the galaxy's bulge. With a ratio of ~1:1000 and with only 0.3 dex scatter, this relation states that the evolution of galaxies and their central black holes are intimately linked (Figure 15). Moreover, this connection requires a mechanism that connects mass build-up in regions different by 10^9 in linear scale.

Another major unresolved issue in present day extragalactic astrophysics is that the late stages of galaxy evolution lack a fundamental understanding: The colour–magnitude or stellar-age–mass diagrams of galaxies show two major populations (Figure 16). In the "blue cloud" of star-forming galaxies a major fraction of the total stellar mass in the universe is created. Most of these galaxies are disks with substantial gas reservoirs. On the other hand, a substantial fraction of this stellar mass will eventually end up in galaxies on the "red sequence" of early type galaxies. Galaxies here are dynamically hot, have little available cold gas, and hence have a low level of or no star-formation at all.

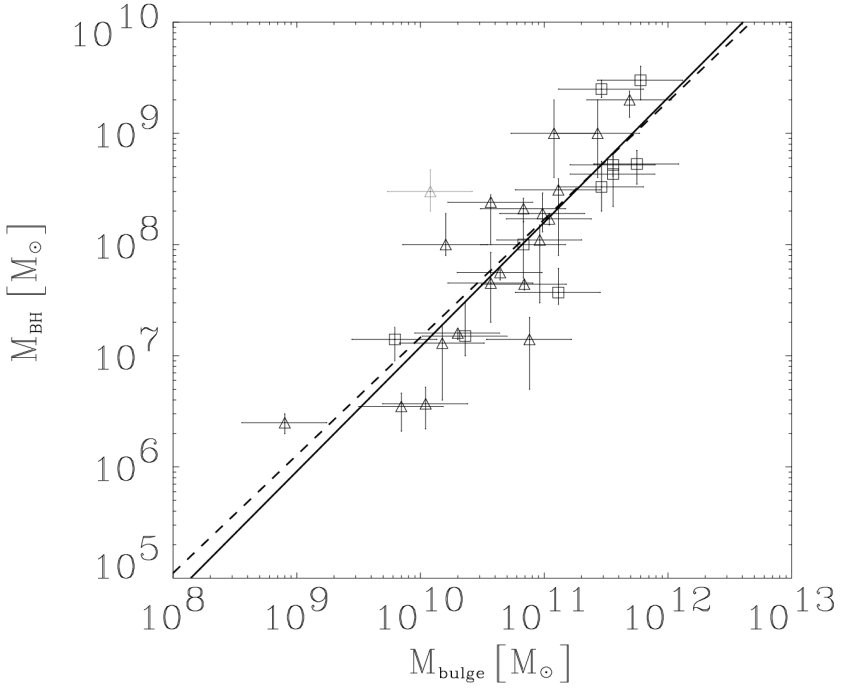

Figure 15: The empirical relation between the masses of nearby galactic bulges and their central black holes. An almost perfectly linear relation is found, with the black hole mass being 0.14±0.04% of the mass of the bulge (at bulge mass 10^{10} M_{sun}). Galaxies and their central black have to co-evolve. From Häring & Rix 2004, ApJ 640, L89.

Both populations are prominent, with a dip between them, containing a mixed bag of galaxies with intermediate properties, with many hosting an AGN. Some are dust-reddened galaxies, some are transition objects. Puzzling is the sparseness of transition objects: If the gas reservoirs of star-forming disk galaxies are used up by continuous depletion via star formation, then the

time a galaxy takes to transverse from the blue cloud to the red sequence would be several Gyr, too long for the two disjoint populations to actually be discernable. With this observation, the existence of the colour bimodality requires a much more rapid truncation of the star-formation for a disk galaxy and subsequent transition to the red sequence on a timescale of order of 1 Gyr.

One of the most plausible mechanisms that would truncate star-formation could be the same mechanism that links the stellar bulge and black hole masses of galaxies: energetic feedback from the supermassive black hole into the galaxy during a phase of strong mass accretion, in short, AGN feedback. The strong accretion or "quasar" phase dominates the mass growth of galactic black holes. The total amount of energy emitted by an active galactic nucleus during such a phase is higher than the gravitational binding energy of matter in its surrounding galaxy. This can a) stop star-formation by heating the gas sufficiently or by physically driving it out of the galaxy, and b) regulate the mass growth in the galaxy in connection with black hole properties.

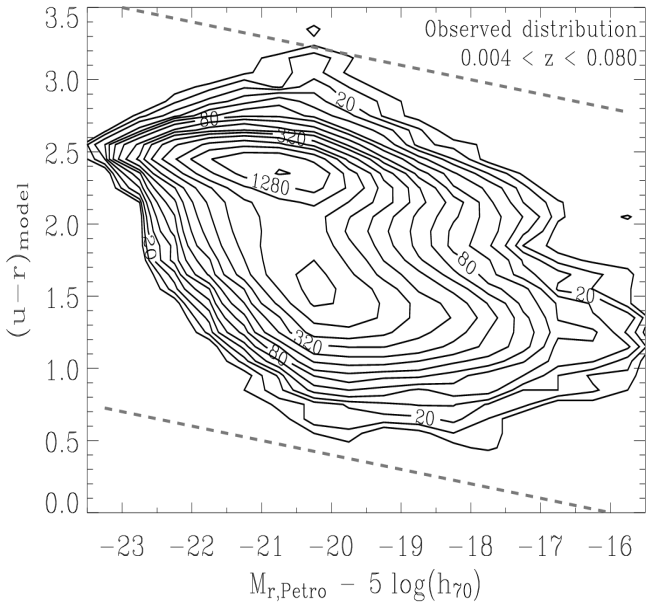

Figure 16: Bimodality in the colour–magnitude distribution of nearby galaxies (higher luminosity runs to the left, colours get bluer upwards). Shown are density contours from ~68000 galaxies in the redshift range 0.004<z<0.080 from the Sloan Digital Sky Survey. The ridge around colour (u-r)=2.5 is the red sequence of early type galaxies, the bluer distribution around (u-r)=1.5 is the "blue cloud" of star forming galaxies. In between lies the "green valley" where the space number density is lower. From Baldry et al. 2004, ApJ, 600, 681.

Numerical simulations of this phenomenon currently lack the spatial resolution to study these mechanisms down to the direct involvement of the black hole, but depending on the exact ad hoc assumptions included, they can result in a major quenching of star-formation on timescales of a few 100 Myr, fast enough for the colour-magnitude bimodality to arise.

Models of the relative growth times of stellar bulge and black hole are also only in their infancy. Depending on the assumptions, different models predict either much more massive black holes relative to the bulges in the past, a moderate evolution in the same direction or no evolution. In the strong cases the mass ratio would have evolved since z=2 and 6 by factors of 2 to 40.

In all cases, a precise empirical determination of the actual bulge mass to black hole mass relation and its evolution since the early Universe needs to be obtained, to constrain the possible physical mechanisms connecting bulge and black hole. The few currently existing studies sample very few targets and do not span a substantial mass baseline. Only two studies reach a redshift of beyond 2.

The only galaxies for which both masses can be estimated are galaxies in the luminous AGN phase, since for broad-line AGN the black hole mass can be estimated using spectral information. This requires galaxy or bulge mass estimates for galaxies with a very bright point source nucleus in their centres at high redshifts; mass-to-light ratios can be estimated using at least one rest-frame optical colour. In addition, an analysis of structure is required to determine the bulge fraction, and an analysis of the dynamical state (i.e. signs for disturbances, interactions or merging) will allow statements about the source for ignition of the AGN itself.

The projected space density of galaxies hosting quasars is already low. Combining all redshifts, there are few per square degree, and even fewer for particular target redshifts. Thus, MICADO being an imager with a field-of-view of >100 kpc at z=2, corresponding to >15 arcsec is a perfect match to observe quasar galaxies individually. Performance requirements for MICADO result automatically from the nature of the targets.

Resolving and measuring properties of the host galaxy around a bright nucleus is not limited by observable depth, but by how well the nuclear light can be characterized in an image. The limits are thus given by a combination of contrast between nucleus and host galaxy brightness, PSF width and the precision to which the PSF shape can be characterized.

We give the example of a host galaxy that contains a 5 times brighter active nucleus. The galaxy is assumed to be spheroidal with r_0=3 kpc at redshift z=3. This corresponds to r0=0.38 arcsec. The PSF used is the latest PSF simulated for the MAORY performance. Here we assume observations in the centre of the field and in the H-band, with 0.8" external seeing. Since the simulated PSFs have a number of sources of unaccounted errors, (LGS cone effect, errors due to the NGS WFS, optics errors and AO calibration errors) this external seeing should give a conservative, yet potentially more realistic PSF for our purpose, than the PSFs computed for the target 0.6" seeing (Figure 17).

The radial surface brightness profiles of the models are shown in Figure 18. The technical objective is to measure the difference between the nuclear emission (black line) and the total emission (green line), with the host galaxy shown as a blue line. In the absence of noise this requires a certain total precision of the nuclear component at each point that corresponds to the ratio of nuclear and galaxy emission. This precision varies as a function of radius for the case where the nucleus is 5 times brighter than the host galaxy (Figure 17): it is directly related to the relative strength of the nucleus compared to the galaxy. A doubling of this ratio will reduce the allowed uncertainty by a factor of 2.

This precision is the product of the precision of the PSF and the precision to which a scaling factor can be inferred, i.e. how well the flux of the nuclear component can be determined. If the radial shape of the PSF envelope is similar to that of the host galaxy, then it is only the core that can be used to infer the relative nuclear point source contribution. In this case the precision will be dominated by the exact knowledge of the Strehl ratio at the location of the QSO at the time of observation. This means we require knowledge of the PSF shape to a few percent.

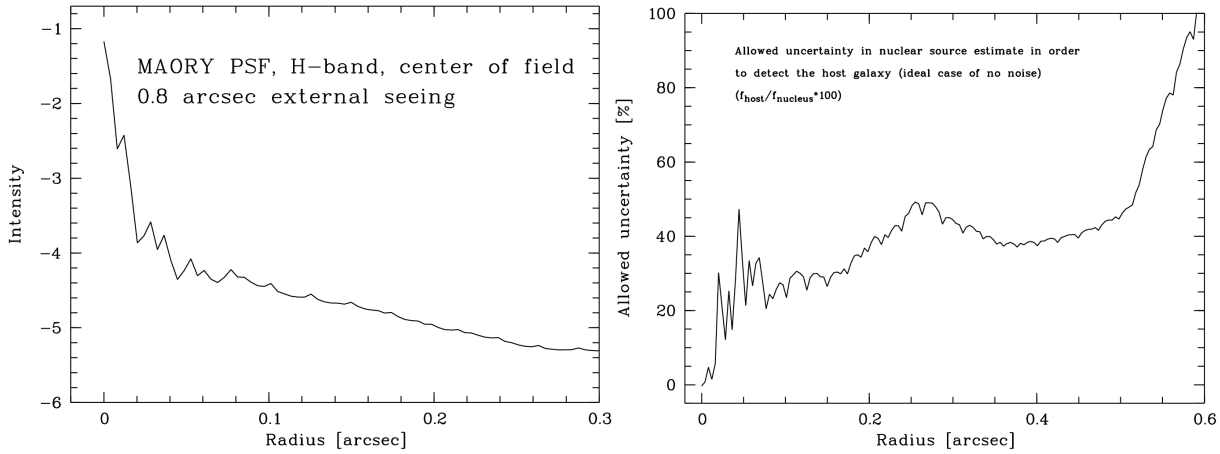

Figure 17: Left panel: radial surface brightness profile of the MAORY PSF. Right panel: allowed uncertainty of the nuclear point source at each point in the noise-free case. This uncertainty is the product of uncertainty in PSF shape and the ability to determine a scale factor.

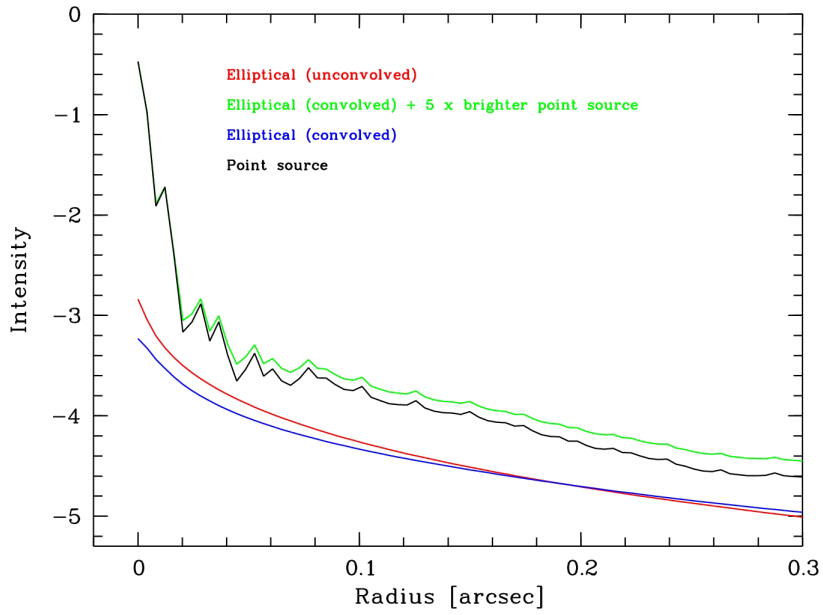

Figure 18: Simulated elliptical galaxy before (red) and after (blue) convolution with the PSF. If a 5 times brighter point source (black) is added, the total profile (green) is produced.

PSF characterization can either be done by inferring the PSF shape from simultaneously observed stars, provided that the PSF is either very uniform, or its non-uniformity is very stable or reproducible from other constraints. Or PSF shape can be potentially reconstructed from wavefront sensor data in the future. This allows for a trade-off between PSF uniformity and stability.

3.5.4 QSO Environments

Quasar environments have been studied on different scales ranging from those of the host galaxy to large scales. Such studies have provided important but controversial results regarding the environment of quasars. It has been known for more than three decades that quasars are associated with enhancements in the spatial distribution of galaxies. These studies have shown that in the nearby universe, quasars reside in environments ranging from small to moderate groups of galaxies rather than in rich clusters (Bahcall & Chokshi 1991b; Fisher et al. 1996; McLure & Dunlop 2001). These findings suggest that quasars are located in high over-density regions, more so than L* galaxies, since higher over-density regions are clustered more strongly than lower over-density regions (e.g. Kaiser 1984; Bardeen et al. 1986). An over-dense environment would indeed be expected if the quasar activity were triggered by galaxy interactions. To develop a better understanding of the quasar phenomenon, it is therefore important to investigate and quantify the relation amongst nuclear activity, host galaxies and the associated environments.

All systematic studies of the properties of QSO environments refer to low redshift ($z < 0.5$) objects. The most extensive studies were carried out by Serber et al. (2006) and Strand et al (2007), based on the SDSS archive. From a large dataset of $z < 0.4$-0.6 quasars, they found that luminous objects are located in higher local over-density regions than typical L* galaxies.

Only for a few selected fields around high-z quasars has the environment been explored (Bornancini et al 2007; Coil et al 2007; Stockton et al 2006). This limitation hinders the possibility to investigate the cosmic evolution of environment and thus to have a full understanding of its role in driving nuclear activity. It is thus of crucially important to study the environments of QSOs at epochs corresponding to the peak of QSO activity and beyond. With the current 8-10m class telescopes this is not possible because inadequate sensitivity and spatial resolution.

In order to be able to observe galaxies of $M > M^*$ at $z=2$-3 it is necessary to detect objects with $K > 24$-25. Assuming a cosmic evolution of the physical radius, these galaxies will have an angular size of 0.2-0.4 arcsec . Under these conditions it is possible to detect these faint ($K \sim 25$) galaxies with integration times of a few hours. The excellent spatial resolution of E-ELT+MICADO will also allow one to detect any signature of interactions for the galaxies closest to the QSO, and thus obtain fundamental data to assess the role of interaction and mergers in the activation and fueling of the QSO phenomenon at the epoch of its maximum.

References

Bahcall, N. A., & Chokshi, A. 1991, in ASP Conf. Ser. 21, The Space Distribution of Quasars, ed. D. Crampton (San Francisco: ASP), 281

Bender et al. 2005, ApJ, 631, 280
Bender et al. 2009, ApJ in press
Bornancini,C.G., Lambas,D.G., 2007, MNRAS 377, 179
Coil, A.L. et al., 2007, ApJ 654, 115:
Lauer et al. 2007, ApJ, 664. L226
Merritt et al. 2007, ApJ, 671, 53
Nowak et al. 2007, MNRAS, 379, 909
Serber et al 2006 ApJ 643 68
Stockton, A; McGrath, E; Canalizo, G., 2006, ApJ 650, 706
Strand, N.E.; Brunner, R.J.; Myers, A.D., arXiv:0712.2474
Tremaine et al. 2002, ApJ, 574, 740
Trippe et al. 2007, MNRAS, 375, 764
Valtonen et al. 2008, Nature, 452, 851

3.5.5 Instrument Requirements

Achieving the highest possible Strehl ratio is critical for accessing the region in nearby galaxies where stellar and gas dynamics are dominated by the supermassive black hole, and for resolving the central QSO/AGN from the host galaxy at high redshifts. While this primarily depends on the performance of the AO module, the requirement on the camera is that it should not degrade in any appreciable fashion the image quality delivered by it. The PSF needs to be 'compact' and well defined; a PSF reference is needed, allowing reliable convolution/deconvolution for which a high photometric accuracy over the field is also required. The FoV of 30 arcsec is largely adequate to explore the central regions of nearby galaxies, and corresponds to ~250 kpc at z = 2.5 (H=70 and concordance cosmology). It is also adequate for the study of the host galaxy and its close environment (< 100kpc) around QSO, where the influence of nearby galaxies is more relevant. However, it would require multiple pointings in order to explore the environment on a wider scale, such as that of proto-clusters and groups at high redshift (e.g., up to 0.5 Mpc projected distance). An instrument configuration that allows the parallel operation of a high resolution imaging channel with the imaging of the full field of view of the instrument would permit exploring the host galaxy and its wider environment using the same observations. For the grism option, a resolution R ~ 3000 is desirable, with simultaneous H and K band coverage.

4 MICADO IMAGE SIMULATOR

In order to evaluate the expected photometric and astrometric capabilities of MICADO we have implemented an image simulator that assumes broad-band filter characteristics and instrument parameters as given in Table 2 Table 3, respectively. Telescope and instrument throughputs (Table 4) are as in the ESO specifications.

Table 2: Parameters for MICADO broad-band filters

Filter	I	Y	J	H	Ks
Central Wavelength (μm)	0.900	1.021	1.215	1.650	2.160
Width (μm)	0.24	0.10	0.26	0.29	0.32
Atmospheric extinction	0.1	0.1	0.1	0.06	0.09
Sky brightness (mag/arcsec^2)	19.1	18.6	16.5	14.4	13.5

Table 3: Telescope and Instrument Parameters

Collecting area		m^2	1275
Throughput	Telescope	%	80
	AO	%	80
	Instrument	%	60-70
	Total	%	39-45
read out noise		e-	5
pixel size		mas	3

Table 4: Assumed Throughputs

Throughput	Y	J	H	K
MICADO	0.65	0.62	0.70	0.61
Total (MICADO+AO+telescope)	0.42	0.40	0.45	0.39

Table 5: Assumptions for the simulated photometry

	I	J	H	K
Aperture photometry (radius, mas)	5	8	10	13
Encircled Energy (aperture)	0.05	0.18	0.30	0.40
Thermal background (fraction of the sky background)	0	0.2	0.4	0.9

One of the most critical parameters is the adopted PSF. For our simulation we adopt the PSF available from the MCAO module consortium:

MAORY http://www.bo.astro.it/maory/Maory/Welcome.html

The optical quality is determined by the convolution between the instrument PSFs and the MAORY PSFs. Given the nominal high strehl ratio of the instrument PSFs over the whole Field of View, for these simulations we have therefore considered only the PSFs delivered by MAORY, shown here in the various panels of Figure 19.

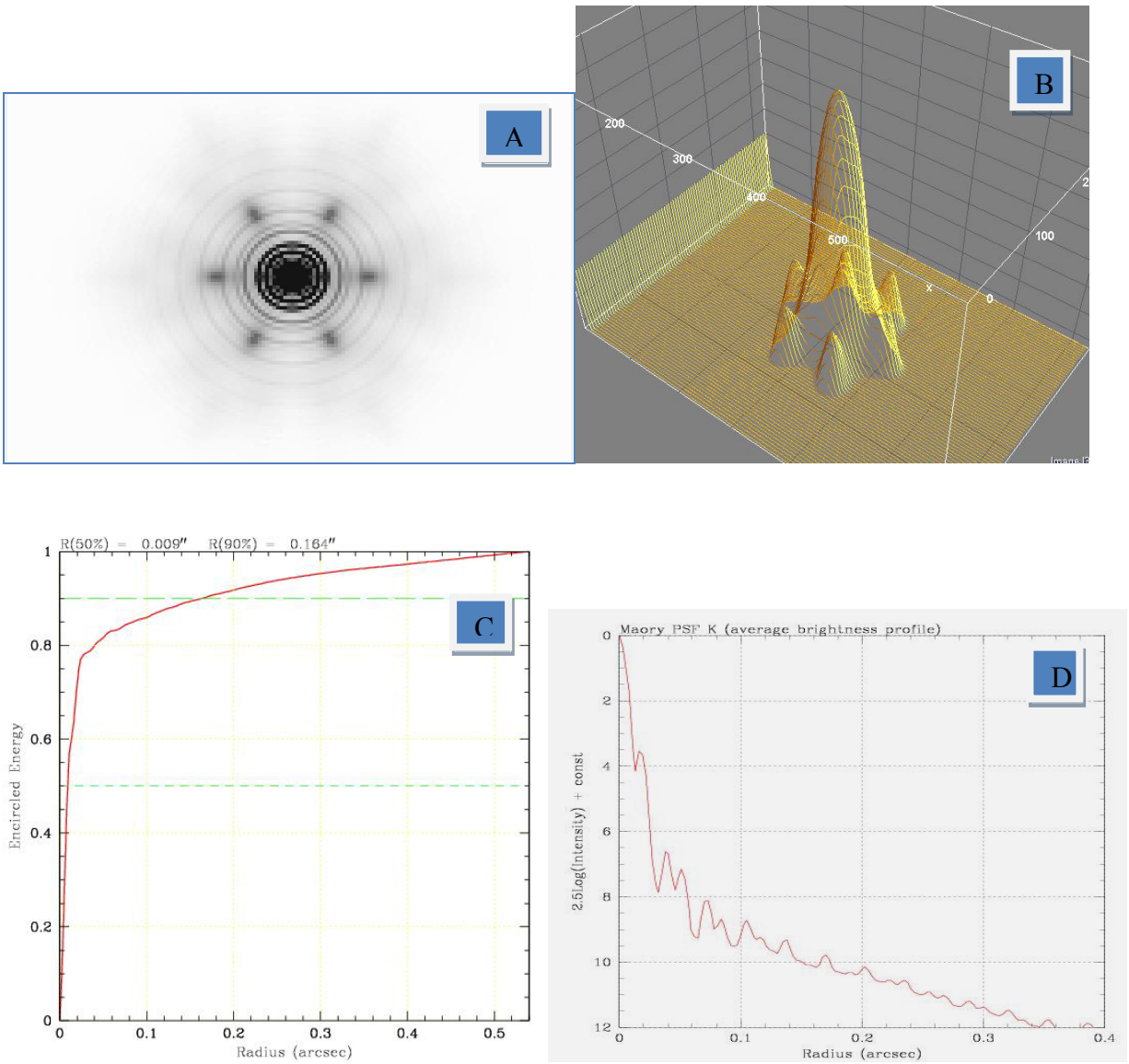

Figure 19 Example of the MAORY adopted PSF in K-band. Image of the PSF core (panel A); 3D view (panel B); encircled energy (panel C); average brightness profile (panel D).

4.1 Magnitude limits for isolated point sources

Figures 20-23 show the expected AB magnitude limits (corresponding to S/N=5, 10 and 25) for isolated point sources as derived under the assumptions reported in Table 5.

The estimated S/N is computed using a circular aperture of radius 6mas (in J) and 13mas (in K). These values represent thus the upper (faintest) limits of photometry of MICADO according with the above specifications. Several effects (smeared PSF, higher background, additional detector noise, …) as well as intrinsic effects of the specific observed field (crowding, underlying nebulosity, …) may combine to degrade the estimated magnitude limits.

An example of crowded field of stars (~7000 stars/arcsec^2), representing the center of a galaxy in the Virgo cluster, is shown in Figure 6. Under these conditions a loss of ~ 1 mag in the magnitude limits results because of the crowding effects.

As a consistency test, Figure 24 shows a comparison of our estimated limiting magnitude with that provided by the ESO ELT ETC under slightly different assumptions.

(Web: http://www.eso.org/observing/etc/bin/gen/form?VIEW.APPLIC.HTM=ins-elt.htm)

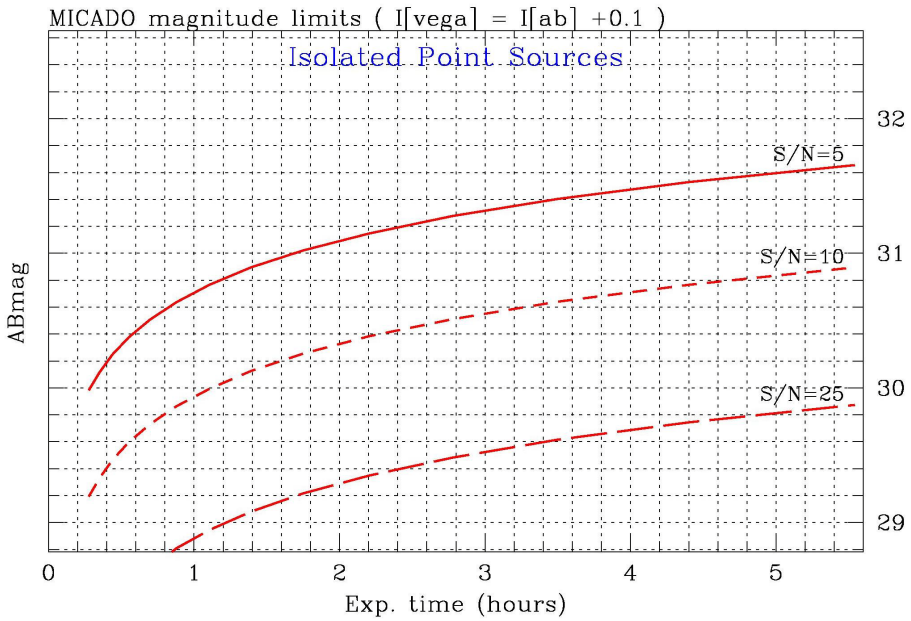

Figure 20 expected I magnitude limit (AB) as a function of integration time of isolated point sources for a signal to noise ratio of 5 (solid line) 10 and 25.

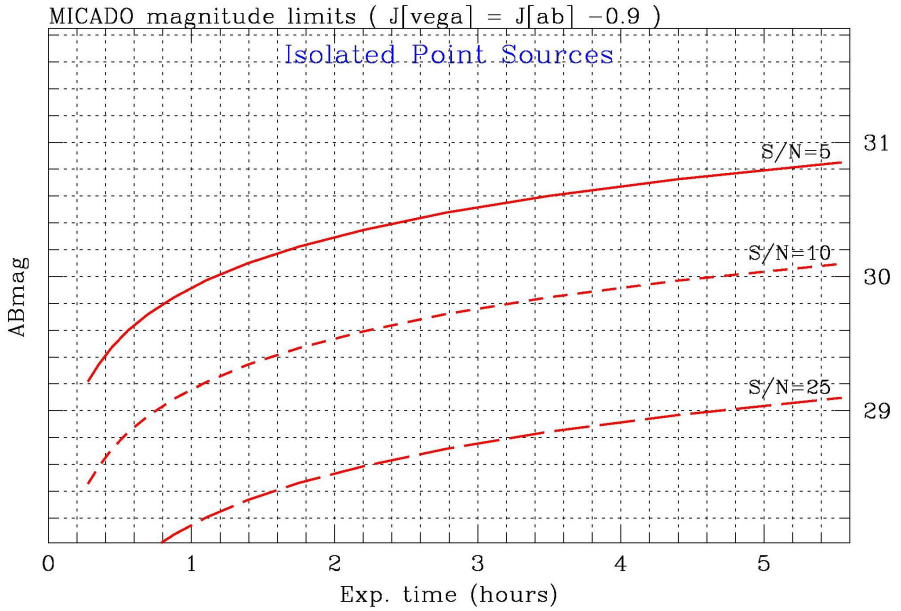

Figure 21 The expected J magnitude limit (AB) as a function of integration time of isolated point sources for a signal to noise ratio of 5 (solid line) 10 and 25.

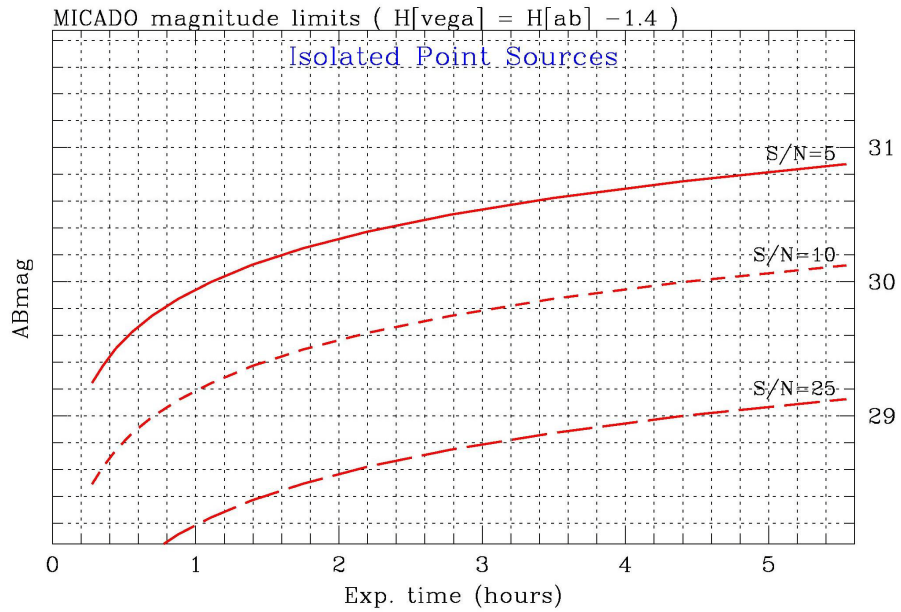

Figure 22: The expected H magnitude limit (AB) as a function of integration time of isolated point sources for a signal to noise ratio of 5 (solid line) 10 and 25.

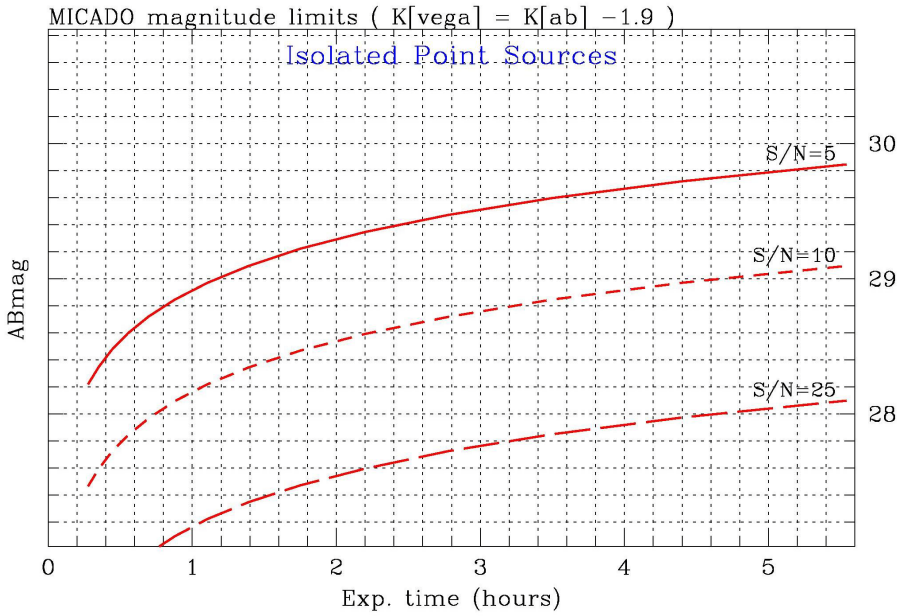

Figure 23: The expected K magnitude limit (AB) as a function of integration time of isolated point sources for a signal to noise ratio of 5 (solid line) 10 and 25.

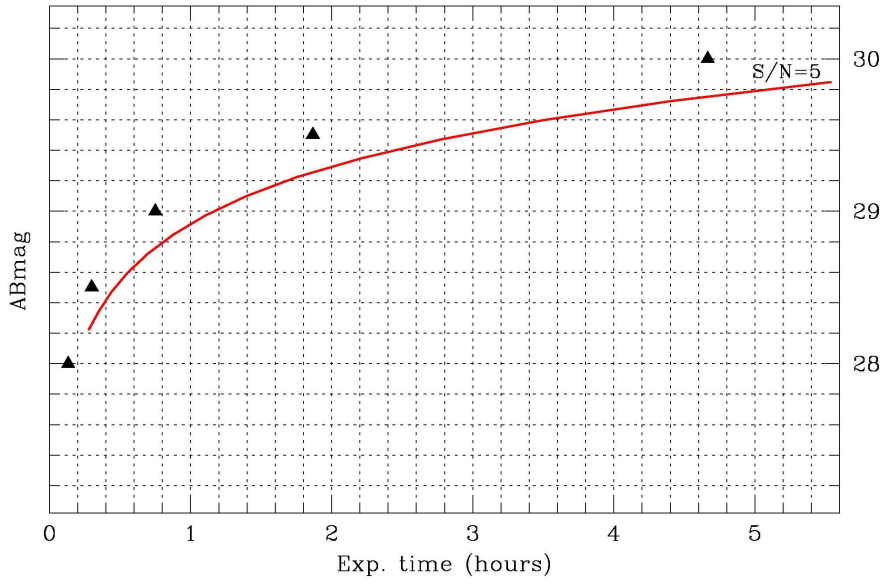

Figure 24: Comparison between our estimate of K (ABmag) limit for point sources at S/N=5 for MICADO (solid red line) with that obtained from ESO-ELT ETC (filled black triangles; using a PSF LTAO, pixel scale 5 mas, RON = 3, SN area 5x5 pix)

Of special interest is the comparison of the expected performance of MICADO with that of JWST. Figure 25 shows such a comparison for the adopted MICADO parameters. It appears that MICADO is nearly as fast as JWST, however over a smaller field.

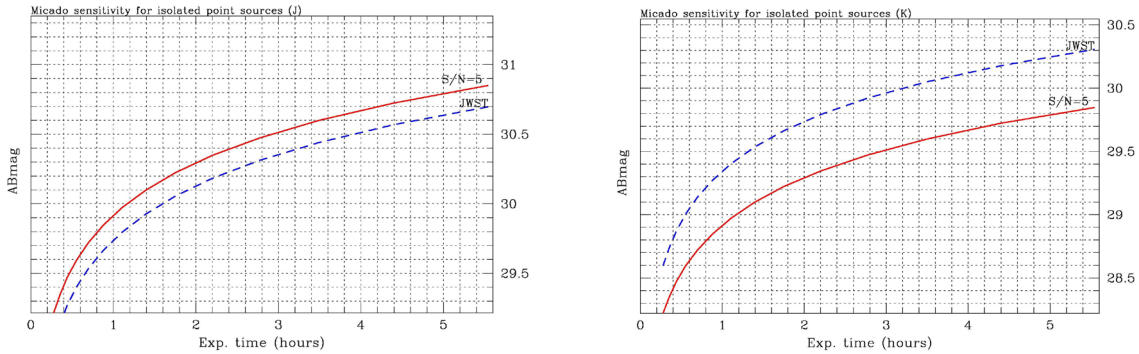

Figure 25: Comparison between the limiting magnitudes in the J and K bands of MICADO and JWST. MICADO appears to be slightly faster than JWST in the J band, and slightly slower in the K band.

4.2 Example 1: A simulated crowded field.

Simulated 3"×3" images in J and K have been produced by randomly distributing stars extracted from the simulation presented in Section 3.3.3, akin to the stellar population in a star forming galaxy. A distance modulus of 31 was assumed, and a high galactic latitude, so that the foreground contamination is negligible. The total number of stars distributed on the images (7000 objects brighter than M_K = -0.8) implies a surface brightness of 21 in the B band, corresponding to the innermost parts of galactic disks. Figure 26 shows the CMD and luminosity function of the injected stars; the residual stellar luminosity (contribution from stars fainter than M_K=-0.8) has not been considered, being well below the sky background. The images, shown in Figures 27 and 28, were analyzed with DOPHOT and the results compared to the input magnitudes. Figure 28 shows that in such a crowded field photometry with an accuracy of 0.1 mag is feasible down to J_{AB}=28, K_{AB}=27, barely reaching the TRGB.

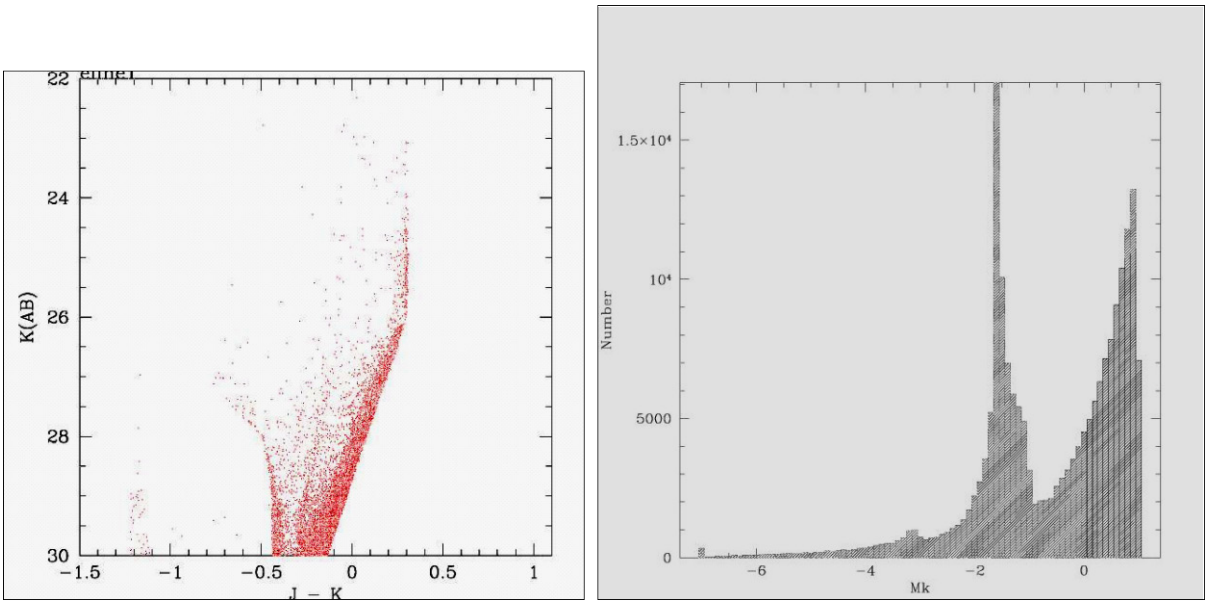

Figure 26: Left: the simulated CMD. Right: distribution of apparent magnitudes in the simulated field.

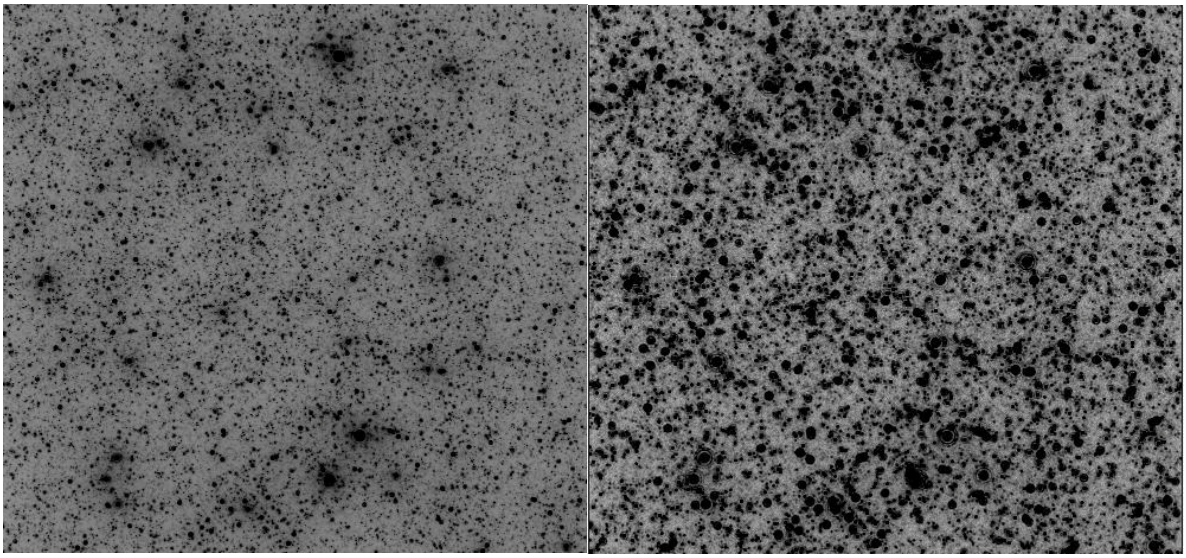

Figure 27: Example of a crowded field (3x3arcsec) in the J (left) and Ks (right) with 5h integration. Due to the higher background in the K band the image of the field is shallower than that in the J band.

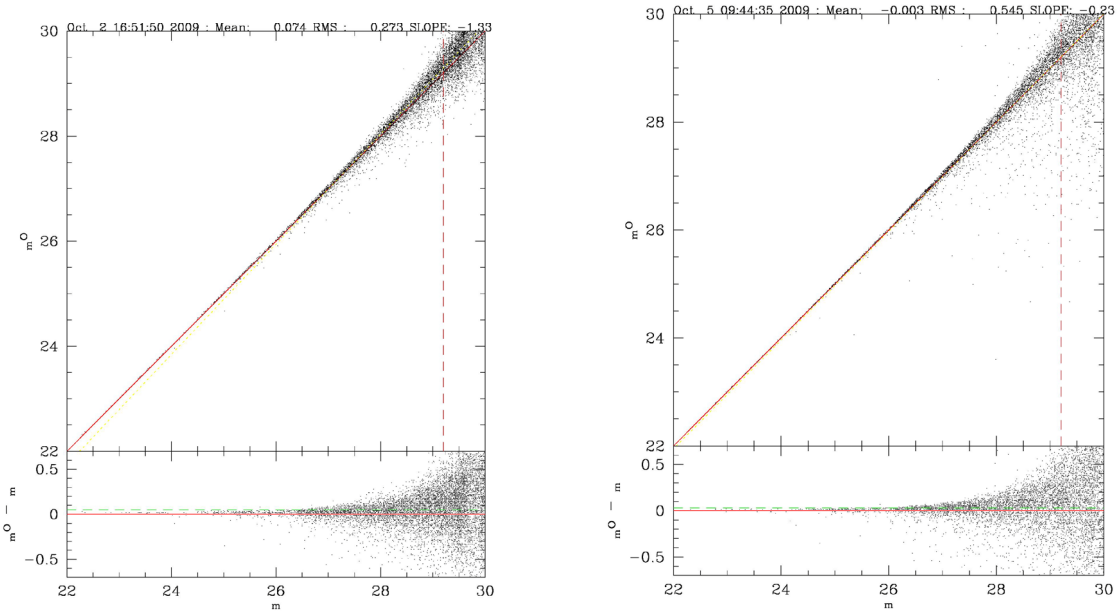

Figure 28: Comparison between the observed magnitude (using DOPHOT) and the simulated (true) magnitude for the crowded field (left: J band; right: K band).

4.3 Magnitude limits for GLAO

The same simulator was used to estimate the performance of a hypothetical MICADO working in Ground Layer Adaptive Optics (GLAO) mode. This assumes a PSF core FWHM of 0.1 arcsec in the K band, and an encircled energy of 30% at twice the FWHM. As illustrated in Figure 29, in such a GLAO mode MICADO would be roughly 2 magnitudes shallower than in the MCAO mode.

Given that MICADO in MCAO mode and JWST have quite similar limiting magnitudes, one concludes that MICADO in a GLAO mode would be roughly 2 magnitudes shallower than JWST.

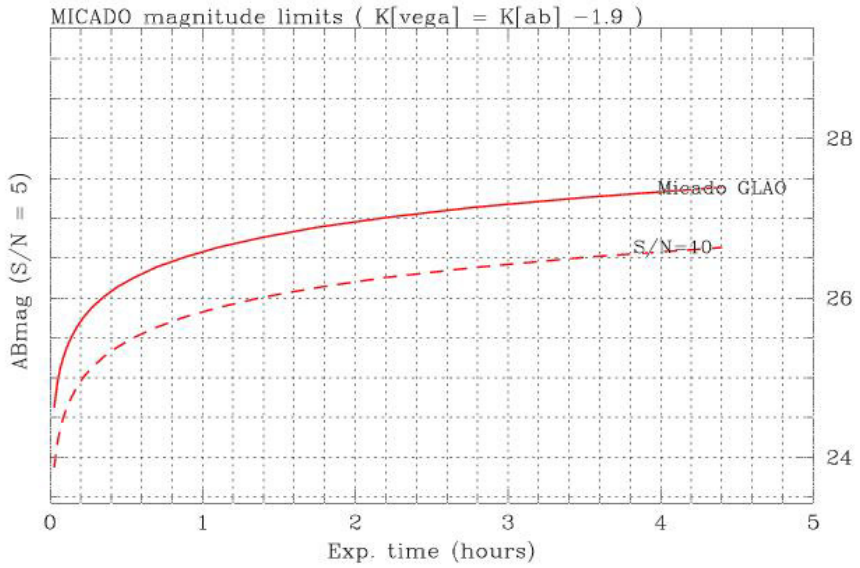

*Figure 29: Estimated magnitude limits in K band for point sources assuming the GLAO case (FWHM of the PSF core 0.1 arcsec; Encircled Energy 30% at R=2*FWHM).*

5 SCIENCE TRADE-OFF

The Trade-Off Table attached to this document synthesizes the MICADO performance requirements from the Science Cases developed by the consortium scientists, some of which are presented in Section 3. It has been used to identify the main science drivers, to provide feedback on the Technical Specifications for the MICADO instrument and update them accordingly, and to prioritize a series of optional modes discussed in this section. In particular, these Science Cases have indicated that it is highly desirable to include in the design an option for the instrument being fed by an SCAO mode, as well as a long-slit spectroscopic mode.

Thus, the Science Cases have helped to identify the instrument design that could satisfy the widest possible scientific needs, while keeping to a minimum the complexity of the instrument itself. This has been achieved thanks to the possibility of adopting different parameters and modes over a portion of the field, such as different pixel scale or inserting additional optical components (e.g. grism, polarizers, Fabry-Perot filter, etc).

5.1 MICADO Optional Modes

5.1.1 Coronagraphy

The question of a coronagraph for MICADO arises when trying to take into account science cases like proto-planetary or debris circum-stellar disks, exo-planets or other, faint structures in the immediate environment of bright stars. Independent of any science case it should be said however, that the performance of any type of coronagraph, be it a classical or apodized Lyot, or an advanced phase-mask-type device (PMC), depends critically on wave front quality, i.e. Strehl ratio. Sivaramakrishnan et al. (2001) have shown that below a Strehl ratio of ~70% no effective suppression of the PSF structure outside of the direct occulting stop can be achieved for Lyot-type coronagraphs. Our simulations in the context of 4 quadrant phase-mask coronagraphs indicate the onset of notable suppression to be around SR~87%. The numbers vary with the exact parameters of the coronagraph (notably with focal and pupil stop diameters and with design bandwidth for a PMC), but generally the minimum required SR appears to be between 70% and 90%.

As a comparison, we quote here the expected numbers for the coronagraph performance of SPHERE, the VLT planet finder instrument, which is expected to achieve SR≈90% in *H*-band:

SR (H-band)		90%
Peak suppression (H)		>100 (goal 400)
Peak suppression (Y)		50
Halo/wing suppression (H)		5-10
Halo/wing suppression (Y)		2

Note that a halo suppression of a factor of 10 increases the contrast effectively by a factor of only $\sqrt{10} \sim 3.2$, because a stable background could be subtracted anyway while the photon noise of the halo would remain. In summary it can be said that for MICADO, no significant reduction of light outside the direct occulting mask area (or of the Airy pattern for phase-mask coronagraphs) is to be expected from any coronagraph because AO system performance is likely to be no better than SPHERE's. However, a coronagraph in MICADO could still serve a two-fold purpose: On the one hand it could block light from an on-axis star and thus avoid detector saturation during long detector integrations. On the other hand, the light blocked by a coronagraph early-on in the optical system cannot be scattered any more downstream of the coronagraph, thus a coronagraph could help avoiding or at least reducing ghosts and stray light problems of bright targets. For these two purposes, a classical Lyot coronagraph would be sufficient – or indeed recommended – because a phase-mask device doesn't block anything.

References

Sivaramakrishnan et al., 2001, ApJ 552, 397

5.1.2 Ground Layer Adaptive Optics

The MAORY's specs are to provide MCAO over a 2arcmin field. The use of just GLAO over a similar field would make sense only if the AO module were largely underperforming, or if no other AO options were available. A purely GLAO mode would make sense only for a field of view largely in excess of the size of the MAORY-corrected field. The following science case was therefore developed to explore the potential performance of MICADO in an extreme GLAO mode of 5'×5' field.

Supernovae with a MICADO Wide-Field option

There are two main scientific drivers for the study of supernovae at high redshift:

- The case for the use of SN~Ia as cosmological probes has been extensively discussed in the literature (Leibundgut et al 2008). The bottom line is that in the last decade, using a sample of few hundreds SNe, most of which in the redshift range $0.5<z<1$, it has been shown that the expansion of the Universe is accelerated, possibly due the presence of a mysterious dark energy. It is argued now that understanding the nature of the dark energy requires enlarging the numbers of SN by an order of magnitude (while also improving measurement and calibration accuracy) and to extend observations to higher redshift, $1<z<2$.
- there is a growing interest for the use of SNe as tracers of star formation history (SFH) and, in general, of the Universe stellar population content with cosmic age (Kouznetsova et al 2008). Conversely, if independent constraints on the SFH are available, measurement of the evolution of SN rate with redshift can be used to discriminate among different progenitor scenarios (Blanc & Greggio 2008). At present, reasonable statistics is available only at medium-low redshift ($z<1$). The few available measurements at higher redshift appear to be in conflict with the current understanding of SFH and SN progenitor scenarios and therefore need to be confirmed.

In the long term the hope is to use SNe to directly probe the outcomes of population III stars. At maximum light, the spectra of SNe of all types, is strongly peaked in the blue bands. This means that at redshift z=1,2,3 the peak emission occurs in bands z,J, H respectively. Therefore to observe SNe at high redshift it is necessary to observe in the near-IR (c.f. Figure 30). In Figure 31, we show, both for SN~Ia and for SN~II, how the apparent J and K magnitudes at maximum change with redshift.

An interesting feature which appears from this plot is that in the redshift 1<z<3 the K apparent magnitude of SN~Ia remains almost constant because the decline of magnitude with the increasing distance is compensated by the progressive shift of the spectral energy distribution peak. However, the magnitude one needs to reach to open this high redshift window is at least 26 mag in K, which is in the reach of MICADO in the most favourable configuration (LTAO) but 2 mag fainter than a possible GLAO configuration.

To evaluate the prospects of MICADO for a possible SN search, we computed the number of events expected, per exposure, both in GLAO and LTAO and compared it with those predicted for JSWT and SNAP (Table).

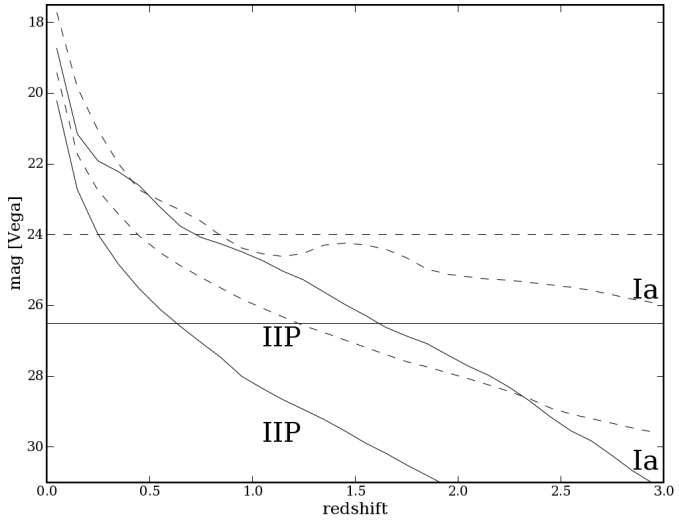

Figure30 Apparent magnitude at maximum as a function of redshift for typical SN~Ia and SN~II in J (dashed line) and K (solid line) bands. Horizontal lines indicate the limiting magnitudes for the LTAO configuration of MICADO. For the GLAO configuration, the limiting magnitudes are 2 mag brighter. Limiting magnitude (Vega system) for point sources, 10-sigma above background, 1h exposure.

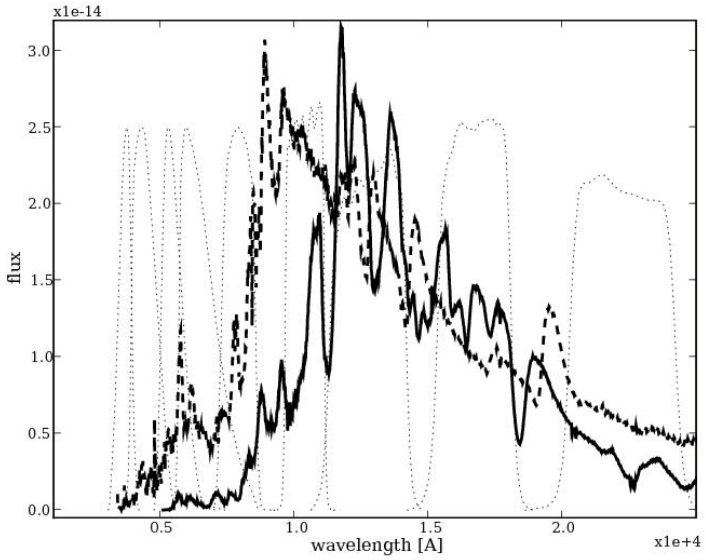

Figure 31: Maximum light spectra of typical SN~Ia (solid line) and SN~II (dashed line) at redshift z=2. Dotted lines show, left to right, the transmission curves of filters UBVRIYJHK

Table 6: Expected SN Ia detection rate (numbers can change by a factor 2depending on the adopted rate evolution model).

Instrument	FoV	J*	SNe/Field		K*	SNe/Field	
			Ia	All		Ia	All
Micado GLAO	5'x5'	25.5	0.2	0.4	24.0	0.02	0.1
Micado LTAO	1'x1'	27.5	0.2	0.8	26.5	0.2	1.2
JWST	2'x4'	30	10	25	28	5	20
SNAP	1°x1°	27	500	2000			

** Limiting magnitudes (AB system) are computed using the E-ELT exposure time calculator (version 2.11), for integrated photometry over a 5x5 pixels of point source, S/N=10, 1 hour exposure. Pixel scale is assumed 50mas/pixel for GLAO and 5mas/pixel for LTAO*

It turns out that in all cases the MICADO detection rate is expected to be a factor 10 lower than with JWST. Also, it appears that the effort to increase the field of view of a GLAO mode is wasted by the shallower limiting magnitude and indeed, despite the smaller field of view, LTAO is expected to be more efficient than GLAO for a high redshift SN search.

We have also to consider that the use of SN Ia as distance indicators requires following the SN luminosity evolution for 30-40 days in the galaxy rest-frame. This implies that it is necessary to obtain accurate photometry of a given SN about 1-2 mag fainter than at maximum light. For a

SN Ia at redshift z~2 this means an apparent magnitude ~29 in J and ~27 in K, which are at the very limit of MICADO LTAO.

In the case of SNAP, a dedicated, relatively small telescope is designed to explore a somewhat lower redshift range ($z < 1.7$). In this case, the key feature is the very large field of view that allows one to explore a huge volume even within a moderate redshift range.

It turns out that for high redshift SN searches a GLAO configuration of MICADO is not competitive. In particular, the gain in field of view is not sufficient to compensate for the expected limiting magnitude which is just 2 mag shallower than what is required to exploit the emission peak in the infrared of high redshift SNe.

References

Blanc, G., & Greggio, L. 2008, New Astronomy, 13, 606

Leibundgut, B. 2008, General Relativity and Gravitation, 40, 221

Kuznetsova, N., et al. 2008, ApJ, 673, 981

Botticella, M. T., et al. 2008, A&A, 479, 49

5.1.3 A Grism Spectroscopic Capability on MICADO

MICADO is one of the simplest scientific instruments currently envisaged for the E-ELT, which makes it an obvious candidate for being chosen among the potential E-ELT first light instruments. The Consortium is therefore making efforts towards a design as simple as possible, keeping to a minimum the number of its observing modes. Yet, while preserving an overall simplicity, relatively minor additions may offer opportunities to greatly enhance the scientific capabilities of MICADO, and therefore of the very early E-ELT itself, if MICADO should be at the telescope from the beginning.

It is for this fundamental reason that the Consortium has considered extremely attractive from a science point of view the inclusion of a simple spectroscopic capability in the current Phase A study of MICADO. Indeed, with a simple, high-throughput long-slit spectrometer one immediately gets the maximum point-source spectroscopic sensitivity of an on-source diffraction-limited E-ELT, surpassing the performance of an IFU for this type of target. This document illustrates how the inclusion of a long-slit spectroscopic option (in the Auxiliary Arm) would enhance the scientific return of MICADO, first for a few scientific applications not mentioned in the Phase-A Scientific Analysis Report (issue 1.1), and then specifically for some of the science cases that have been developed for the imaging mode of the camera and described in the mentioned document.

Prominent examples of cutting-edge applications of a long-slit mode may include the following:

- Obtain emission-line spectra (hence redshifts, velocity widths, metallicities, etc.) of candidate z>6 starburst galaxies that would be identified photometrically.
- Get spectra of the highest redshift supernovae (from z~1 to z>>1), measuring their redshifts, determining their SN Type, and checking for systematics in spectral properties

with respect to local supernovae (a critical test for the use of Type Ia supernovae as standard candles).

- Get absorption line spectra of the first (apparently very compact) elliptical galaxies that formed at z~3-2. Critical is measuring the central velocity dispersion of these galaxies, which is currently well beyond the capabilities of 8-10m telescopes.
- Get emission line spectra of individual star-forming clumps/HII region complexes in galaxies at z ~1–5. The crucial measurements are line ratios, line widths, and velocities relative to the systemic velocity in order to measure their dynamical masses, map their morphological/kinematic substructure, determine their SFRs, metallicities, gas/dust contents, search for outflows and intermediate mass black holes. This requires high angular resolution and sensitivities that will only become possible with ELTs and diffraction-limited instruments.

The Galactic Centre

The science case is extensively illustrated in Section 3.1 of the Science Analysis Report, including the opportunities offered by a long-slit option. Here the main advantages of combining the astrometric and spectroscopic capabilities of MICADO are reported.

- Determination from both astrometric data and Doppler spectroscopy of the orbits of fainter (K≤20-21) main sequence stars in the inner cusp, with semi-major axes significantly smaller than the current S-stars. Extrapolations from the surface density distribution and K-band luminosity function indicate that one can expect ~5-10 stars with K≤20 (m≥1.4 $M_{\odot}$) in the innermost 0.1-0.2", of which a few stars may have peri-bothroi $<10^3$ R_s, several times smaller than that of S2. Such stars would have orbital time scales of a few years. In this case the Schwarzschild precession term and other GR terms will be detectable in a decade of observations.
- Study the central accretion zone surrounding SgrA*. With the resolution of the EELT (5-10 mas) it will be possible to study in detail the spectral and temporal properties of accretion events and search for evidence of outflows/jets predicted for radiative inefficient accretion flows as in the Galactic Centre. Short term astrometry within an accretion event as well as the search for positional shifts between accretion events at different times are of great interest for determining evidence for orbital motion and outflow of the hot gas, as well as the predicted Brownian motion of the central massive black hole.

The central structure and supermassive black holes in nearby galaxies

Section 3.5 of the Science Analysis Report presents the MICADO science case for the study of the nuclear regions of nearby galaxies. The availability of a long-slit (8") grism spectroscopy mode through the Auxiliary Arm would highly enhance the science output of MICADO. This is especially the case for the study of the nuclear regions of nearby galaxies, as the stellar kinematics of the (unresolved) centres of galaxies could be measured with unprecedented

accuracy and proximity to the supermassive black hole. A spectral resolution of R~3000 for a 10 mas wide slit is needed to avoid the sky lines in the K band and resolve the typical velocity dispersions at the centres of (spiral or low-luminosity) galaxies. With such configuration one would have σ_{instr}~40 km/s, or ~15 km/s per pixel with the 1.5 mas pixel configuration. An even better sampling, ~15 km/s per pixel, would be achieved if 1.5 mas pixels were available. Nodding the slit some 2 arcmin away from the target will be needed to get sky spectra. Spectral dithering, similar to what is available in SINFONI, would enable the measurement of velocity dispersions as low as 20 km/s.

With this spectral resolution, Figure 14 shows the sphere of influence of a black hole of a given mass as a function of angular distance. Here we use the Tremaine et al. (2002, ApJ, 574, 740) relation to link black hole mass to velocity dispersion and we show galaxies with black hole mass determinations from stellar and gas kinematics. At the moment direct measurements are lacking at the low σ end, and are essentially limited to local galaxies. MICADO will be able to spatially resolve the dynamical influence of "seed black holes" in local inactive bulge-less or dwarf galaxies (using the rest-frame CO band heads in the K-band out to ~50 Mpc) and the supermassive ones of inactive massive ellipticals out to redshift z~0.35 (using the rest-frame H-band). Assuming that sensitivities comparable to SINFONI will be achieved, the increase in collecting power of E-ELT compared to the VLT compensates ¼ of the flux reduction due to the increased resolution in case of constant surface brightness. Thus, from SINFONI experience (e.g., Nowak et al. 2007, MNRAS, 379, 909), confirmed by the use of the ELT spectroscopic exposure time calculator, one expects to reach high-enough spectral S/N ratios to derive stellar kinematics with integration times of the order of 10 hours for local dwarf ellipticals or low-luminosity bulges.

For the case of local bright ellipticals, where SINFONI observations require ~8 hours exposure time, several nights of integrations would be needed to compensate for the distance of z~0.35 objects. Note that these science cases exploit the observed K band, where the maximum Strehl ratio is achieved. The availability of a larger spectral range at the same spectral resolution (through a 'linear' alignment of the detectors) adds to the science results by increasing the effective spectral signal-to-noise ratio only if the achievable Strehl ratio (and therefore overall spatial resolution) at shorter wavelength is above 20%. This will be probably true only for the H band, therefore the present science cases would profit from an H+K simultaneous coverage, but not from further extensions to shorter wavelengths. The slit length of 8" is well matched to the science case, in combination with a 2 arcmin nodding strategy. A smaller length down to 4" would be also feasible.

Intermediate mass black holes in globular clusters

Deep MICADO imaging of globular clusters is one of the astrometric science cases in the Science Analysis Report (Section 3.2), and would be aimed at measuring parallaxes and proper motions of these objects. A by-product of such observations will be the possible discovery of cluster stars having been accelerated to very high velocities while in a close passage near an intermediate mass black hole. Prompt spectroscopic follow-up of such stars would allow one to measure the mass of the black hole with much greater accuracy than possible solely with astrometric measurements.

Stellar populations in galaxies up to the Cen A Group

The photometric application for the study of resolved stellar populations in galaxies up to Virgo is the object of the science case presented in Section 3.3 of the Science Analysis report. Here one briefly illustrates the advantages for this scientific area of a spectroscopic option for MICADO.

Abundance ratios, in particular the alpha-elements to iron ratio, has proved to be an important tool in setting constraints on the timescale of star formation in old stellar systems, such as the Galactic bulge, halo and thick disk. Similar studies have been attempted at Keck for M31, but failed because of insufficient S/N in the DEIMOS spectra. With a long slit spectroscopic option and sufficient resolution (R~10,000) MICADO would make possible these studies all the way to the distance of the Cen A group (~3.8 Mpc), hence allowing the measurement of the alpha/Fe ratio of stars in a true elliptical galaxy. This would be of great significance for the calibration of alpha/Fe estimates from integrated light observations and stellar population synthesis. In the near-IR there exist several lines (FeI, MgI, SiI, TiI, CaI, CO, and OH) from which the abundance ratios can be derived (e.g., Origlia et al. 2005, MNRAS, 356, 1276).

Instrument Requirements

From the above science cases, one derives the following main requirements for the spectroscopic option for MICADO.

- Spectral Resolution: R=3000 is adequate for most applications and sufficient to cope with the sky lines. However, R ~ 10,000 (or better) is required for studies of stellar abundances.
- Slit Length: the full width of the Christmas Tree field of view (8")
- Slit Width: 10 mas (multiple slit width options may be desirable)
- Pixel scale: 2 mas (a 1.5 mas option may be desirable)

Instrument Performance

We have developed a simple ETC (that appears to give consistent results with the ESO-based ETC). Using the following assumptions: R=3000, slit width=10mas, efficiency of the spectroscopic elements 50%. The other parameters (telescope and MICADO throughputs) are the same as those specified in the imaging mode (see Section 4 of this document). The S/N is computed per resolution element. In the case of K band the thermal background is added to the sky background (assuming the two components are similar). The resulting magnitude limits as a function of source integration time for various S/N values (per resolution element) are given in Fig, 32 and Fig. 33, respectively for the K- and the J-band.

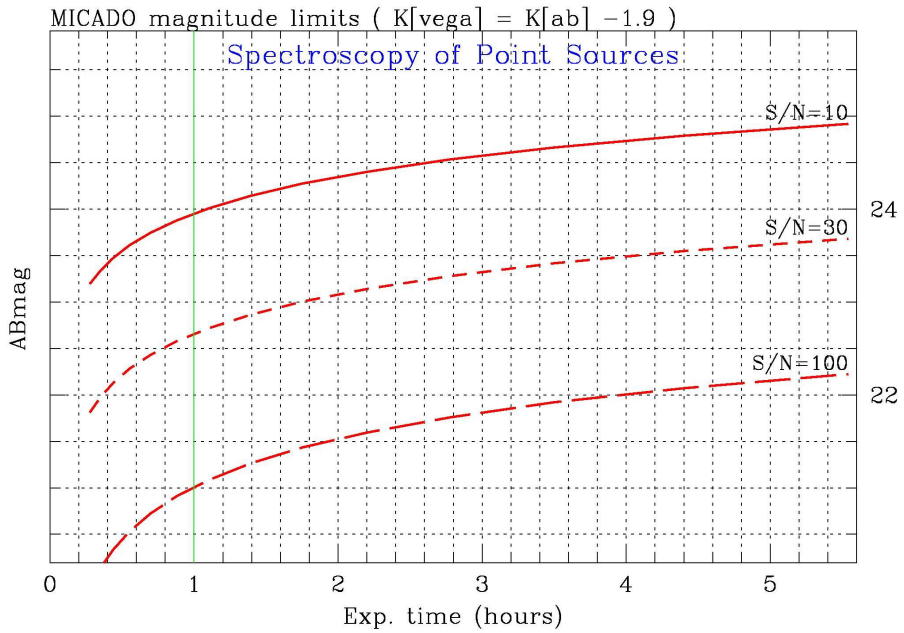

Figure 32. The limiting K-band magnitude for point sources of the spectroscopic mode (R=3000; slit=10mas) as a function of on source integration times for various S/N values(per resolution element).

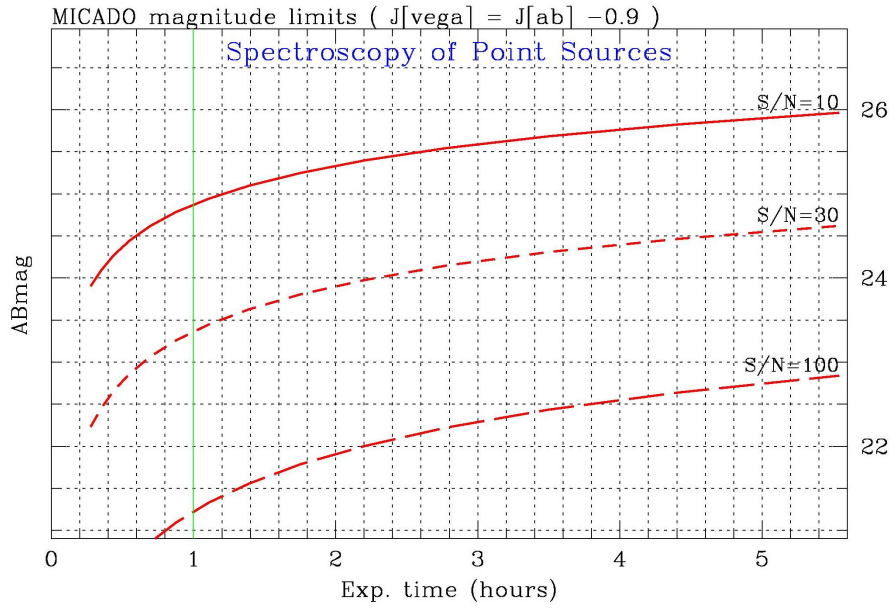

Figure 32: The limiting J-band magnitude for point sources of the spectroscopic mode (R=3000; slit=10mas) as a function of on source integration times for various S/N values(per resolution element).

5.1.4 Polarimetry

A polarimetric capability can facilitate a number of the mentioned science cases along with additional ones. Here we differentiate between imaging- and spectro-polarimetry. We list a number of current day polarimetric science topics that would benefit from an appropriate polarineter being installed on MICADO.

Imaging:

- Observations of flares around Sgr A* to determine orbits around the Milky Way black hole (e.g. Meyer et al. 2006, A&A, 458, 25)
- Jet geometry and physics in X-ray binaries (Russel & Fender 2008, MNRAS, 387, 713)
- Cometary dust grain compositions and comet fragmentation (Jones et al. 2008, AJ, 135, 1318)
- Frequency of disks around young stellar objects (Jiang et al. 2008, ApJ, 673, 175)

Spectroscopy:

- Identification of obscured quasars at high redshifts by finding broad-line signatures in reflected light (e.g. Zakamska et al. 2005, AJ, 129, 1212)
- Analysis of the environmental geometry of SNs (Chornock et al. 2006, PASP, 118, 722)
- Geometry and outflows around high redshift Ly-alpha emitting galaxies, including possible OH-suppression of atmospheric lines by polarisation (e.g. Dijkstra & Loeb 2008, MNRAS, 386, 492).

In summary, a polarimetric capability for both imaging and spectroscopy over a fraction of the instrument field of view is worthwhile and has the potential to facilitate very interesting science that the extremely high collecting area of the E-ELT would make possible with adequate S/N for the first time.

5.1.5 Simultaneous Colour Imaging

Early in the Phase A study, the science team considered the option of including simultaneous multi-colour imaging, and the engineering team looked at how this might be implemented. The importance of the technique to each of the main science cases was assessed and is shown in the Trade-Off table in the Appendix. The only 2 science cases to consider it highly important both have compact targets (i.e. field of view is not considered important, and would be traded off in favour of smaller pixels) and require detailed knowledge of the PSF (in order to separate it from the surrounding extended emission). The Galactic Center science case also favoured the technique, but with the aim of improving the photometry.

The rationale for using simultaneous multi-colour imaging is that perhaps one can acquire better knowledge about the PSF – specifically from the way in which adaptive optics performance scales with wavelength – in order to improve PSF subtraction and photometry. However, this is in fact a rather complex issue, particularly when the AO correction is done using multiple natural and laser guide stars. The implicit assumption is that some level of PSF

reconstruction using WFS data is possible, but that is considered a significant challenge by AO groups.

Ultimately, the science team concluded that the technique might lead to some benefits, and perhaps should be considered for an instrument designed specifically for single-conjugate AO over a small field of view. However, given a finite number of detectors and the fact that MICADO is optimized for multi-conjugate AO, the majority of the science cases are better served by imaging a large field in a single shot. This improves the spatial uniformity of the PSF since it removes the issue of differential temporal variability.

5.1.6 Tunable Filter

The science driver for a tunable filter has been described in Section 3.4.4 in the context of emission line mapping of high redshift galaxies. In this context, it is important to understand not only emission line flux, but also the distribution of the emission lines. It is for this reason that integral field spectrometers were developed. However, because they have a large wavelength coverage, their field of view is severely limited. The alternative is the use of a Fabry-Perot etalon. FP etalons have a distinct advantage in terms of spatial pixel sampling and field coverage, both of which tend to be compromised with other techniques (e.g. integral field spectroscopy) in order to gain spectral coverage. Specifically, such devices offer the only viable way of generating emission line maps at the diffraction limit of the E-ELT and covering a field of view of 1arcsec or more. For high redshift galaxies, because one is interested in only specific emission lines rather than the full spectrum, FPs offer a very enticing option.

However, their efficacy has been limited by temporal variations in the atmosphere (most importantly the seeing), which make it very difficult to subtract the continuum image to reveal the line emission. In order to develop an FP that is scientifically productive – and that will be used by the community – we need to overcome this problem, and at the same time ensure that the FP meets the science requirements (resolution, wavelength stability across the field) and has a functional pipeline to process the data

The basic requirements for such a filter are very demanding and would require a dedicated study. They are that it

(i) should provide a bandpass of 500-1000km/s

(ii) can be tuned anywhere in the J-K bands,

(iii) images a field of view of several arcsec while sampling the diffraction limit

(iv) both emission line and neighbouring continuum wavelengths are imaged simultaneously

The science team considers this a potentially very interesting capability that could provide significant science return. As such, we propose to carry out a detailed study of this option during MICADO's Preparatory Phase (see also Section 3.2.4.1. of RD6) so that we can reach a decision about whether it can and should be included before the start of Phase B.

5.1.7 High Time Resolution Astronomy

The science that can be addressed use fast time resolving detectors includes:

- Emission processes associated with compact objects – neutron stars, white dwarfs and black holes;
- Stochastic behaviour in accretion disks around white dwarfs, neutron stars and black holes;
- Stochastic behaviour in pulsar magnetospheres – optical/IR counterparts to rotating radio transients and giant radio pulses;
- Follow-up observations of gamma (and other) ray burst transients;
- Time resolved IR observations of magnetars – Anomalous X-ray Puslars and Soft Gamma Repeaters.

These phenomena are examples of extreme physics mentioned in the road map for European Astronomy, although they do not represent by far an exhaustive list. These objects can be studied in the optical, where most current HTRA observations are made, and in the future in the infrared. In the context of the E-ELT, HTRA observations in the near-infrared over the wavelength range 0.8-2μm would make a significant impact on all of these science areas [1,2]. For example in pulsar magnetosphere studies, it is in the near-IR that we expect to see evidence of synchrotron self absorption, which will severely constrain the local magnetic field around the emission zone. The E-ELT would be expected to be able to observe most of the Fermi gamma-ray pulsars – increasing the number of detections from 5, a curiosity, to more than forty, the start of a survey. Time resolved observations are vital to these studies as, for example, time averaged fluxes give misleading estimates of even the luminosity for time varying objects [4]. For more science details see the two Opticon funded publications references 3 and 5.

In summary, a high time resolution capability is a worthwhile option exploring during MICADO's Preparatory Phase (i.e. before Phase B begins) for the Auxiliary Arm for both scientific and technological reasons: (i) this would provide an additional unique capability that is not foreseen for any other ELT; (ii) it might be possible to incorporate such a device with very little impact on the overall design of the arm since to a large extent all that is needed is a movable pickoff mirror and an appropriate detector (see Section 3.2.4.2 of RD6).

References

1. Shearer A., et al., 2008, Proc. SPIE, 6986, High time resolution astrophysics and ELTs: Which wavelength?

2. Shearer A., et al., 2008, in High Time Resolution Astrophysics: The Universe at Sub-Second Timescales, 984, 232, High Time Resolution Astrophysics and Extremely Large Telescopes

3. Phelan et al., 2008, in High Time Resolution Astrophysics: The Universe at Sub-Second Timescales, AIP Conf. Proc. 984

4. Shearer, Andrew, 2008, Astrophysics and Space Science Library, 351, 4020, High Time Resolution Astrophysics and Pulsars

5. Phelan, Don, Ryan, Oliver, and Shearer, Andrew, 2008, Astrophysics and Space Science Library, 351, High Time Resolution Astrophysics

6 APPENDIX: SCIENCE TRADE-OFF TABLE

E-ELT * MICADO TradeOff Table | Version 2008 13-Feb | **Last rev:** 11.21.08 1:33 PM

MCAO science case	Title	Galactic Center	High-z resolved colour mapping	high-z emission line mapping	Globular cluster astrometry	Star formation histories	QSO environments	Globular cluster photometry	Galaxy Cores	Dwarf Spheroidal Kinematics	Structure of High z Galaxies	deep, faint photometry	QSO host galaxies at high z	YSO's, outflows, disks	High-mass SF
	Lead author; co-authors, Institute	*R. Genzel MPE*	*TBD*	*TBD*	*G. Piotto UnivPD*	*L. Greggio Inaf OAPD*	*R. Falomo Inaf OAPD*	*G. Piotto UnivPD*	*Bender, Saglia MPE*	*K. Kuijken*	*Marijn Franx*	*E. Tolstoy*	*H.-W. Rix, K. Jahnke*	*T. M. Feldt, Herbst*	*T. Herbst, M. Feldt*
Instrument spatial parameters	is 30" FoV ok? if not, what?	yes	yes	yes	Yes	Yes	Yes	60"	yes	yes	pref 60"	yes	yes	yes	yes
	are 3mas pixels ok? if not, what?	2mas	yes	yes	Yes	Yes	Yes	Yes	yes	yes	yes	yes	yes	yes	yes
	is a detector gap of 150pixels ok?	yes	yes	yes	Yes	Yes	Yes	Yes	yes	yes	yes	yes	yes (1)	yes	yes
	is a detector gap of 500pixels ok?	yes	yes	yes	Yes	Yes	Yes	Yes	yes	yes	yes	yes	yes (1)	yes	yes
	preference for wider field or smaller pixels	Small pixels	Wide field	Wide field	Wide field	Small pixels	Small pixels	Wide field	Small pixels	small pix	wide field	small pix	small pix	small pix	small pix
	finer sampling needed at λ<1um? if so, what?	N/A	No	No	NO	NO	NO	NO	NO	2mas	no	2mas	no	yes (see below)	no
Instrument spectral parameters	short wavelength (in range 0.6 1.0um)?	1.00	0.60	0.80	1.00	0.60	0.80	0.60	1.00	0.80	0.80	0.60	1.00	0.8 would be nice	1.00
	importance of simultaneous multi-colours (1=low; 5=high)	4	3	3	1	3	1	3	2	1	2	2	5	5 (SDI only!)	2
Filters	essential filters	H K	ZYJHK	<1% narrow band	YJHK	IJHK	NB	IzJHK	JHK	JK	ZYJHK	IK	J H K	JHK + all std NB, 20+ slots	JHK + all std NB, 20+ slots
	optional filters		I	N/A	1% NB	R	ZJHK	R	none	I	?	V	I	I	?
Technical science drivers	importance of photometry (1=low; 5=high)	4	3	3	3	5	3	5	4	3	3	5	3	3	3 (5 for TM)
	photometric accuracy required	0.05mag	<0.03 mag	<0.03 mag	<0.05	0.03	<0.1	<0.01	0.05 mag	0.05	0.1	<0.01	0.05mag	0.05mag	0.05mag (0.01 for TM.)
	importance of astrometry (1=low; 5=high)	5	1	1	5	2	1	4	4	5	1	4	1	5	5
	astrometric accuracy required	<100uas	N/A	N/A	50uas	N/A	N/A	<100uas	<100uas	0.1mas	N/A	0.1mas	N/A	100uas	100uas
	importance of sensitivity (1=low; 5=high)	3	5	5	5	5	5	5	3	1	5	5	3	4	4
	importance of spatial resolution (1=low; 5=high)	5	5	5	5	5	5	5	5	5	5	5	5	5	5
	importance of fidelity (PSF uniformity) across field (1=low; 5=high)	4	4	4	5	4	3	5	4	4	4	5	5 (2)	5 (3)	5 (over 10as), 3 (full field)
PSF calibration	importance of having a PSF reference (1=low; 5=high)	3	4	4	2	1	4	1	4	1	3	3	5	3	5
	accuracy of PSF required	5%	10%	10%	?	?	?	?	5%	self-cal	10%	5%	5% (at each pixel)	1% EE	5% EE
	importance of having PSF provided by AO software (1=not at all; 5=crucial)	2	3	3	1	1	2	1	4	2	3	3	4	2	2
	PSF characterisation: strehl, FWHM, or encircled energy?	strehl	FWHM, EE	FWHM, EE	Strehl	en. ener.	en. ener.	Strehl	strehl	strehl	en. Ener.	strehl	structure, EE	structure	FWHM, Strehl
Impact of science case	with good AO: 50% strehl at K (1=low; 5=high)	5	5	5	5	5	4	5	5	5	5	5	5	5	5
	with moderate AO: 30% strehl at K (1=low; 5=high)	4	4	4	4	3	4	4	4	4	4	4	4	3	5
	with poor AO: 10% strehl at K (1=low; 5=high)	2	3	3	3	2	3	3	3	2	3	3	2	1	3
Impact of other telescopes on science case	operational TMT (1=low; 5 =high)	5 (if in south)	4	4	3	2	4	4	5	2 unless >>30m	4	3	2	5	5
	operational GMT (1=low; 5=high)		3	4	1	1	2	2	4	2 unless >>30m	3	2	2	5	5
	operational JWST (1=low; 5=high)		1	1	3	5	5	5	3	1	1	5	4	complementary, no conflict	complementary, no conflict

E-ELT * MICADO TradeOff Table	Version	2008	13-Feb		Last rev:	11.21.08 1:33 PM

MCAO science case	Title	Galactic Center	High-z resolved colour mapping	high-z emission line mapping	Globular cluster astrometry	Star formation histories	QSO environments	Globular cluster photometry	Galaxy Cores	Dwarf Spheroidal Kinematics	Structure of High z Galaxies	deep, faint photometry	QSO host galaxies at high z	YSO's, outflows, disks	High-mass SF
	Lead author; co-authors, Institute	*R. Genzel MPE*	*TBD*	*TBD*	*G. Piotto UnivPD*	*L. Greggio Inaf OAPD*	*R. Falomo Inaf OAPD*	*G. Piotto UnivPD*	*Bender, Saglia MPE*	*K. Kuijken*	*Marijn Franx*	*E. Tolstoy*	*H.-W. Rix, K. Jahnke*	*M. Feldt, T. Herbst*	*T. Herbst, M. Feldt*
Additional Questions	how useful would a coronograph be (1=not at all; 5=very)?		2	1	1	1	3	1		1			1		
	how detrimental are image distortions (1=not at all; 5=very)		2	2	5	2	2	2		3					
	would you prefer less image distortion if it means 10% less throughput?		No	No	Yes	NO	NO	NO		yes					
	impact of case with LTAO, i.e. only a small corrected field (1=low ; 5=high)?		3	1	5	5	1	4		4					
	if multiple pixel scales are available, which would be useful: 1, 2, 3, 4, or 5mas/pix		3,4,5	3,4,5	2.4	2.4	2.4	2.4		2,4					
	is zooming over central channel enough; or is it needed over the whole		Enough	Enough	Enough	Enough	Enough	Enough		enough					
	uniformity of PSF across field: what is largest acceptable relative change in strehl (or encircled		10%	10%	10	10	10	10	20 if smooth						
	would you be willing to trade some AO performance for increased PSF uniformity?		Depends	Depends	Yes	Yes	NO	NO		no					
	what is the minimum acceptable sky coverage: 40, 60, or 80%		40%	40%	40	40	40	40	total area counts						
	would you be willing to trade some AO performance for increased		No	No	NO	NO	NO	NO		no					

NOTES	
TM	Transient Monitoring
EE	Encircled Energy
"(1)"	if PSF determination is not affected
"(2)"	unless PSF can be determined at each point from external data
"(3)"	if PSF refefernce existing, 2 (if not)

---oooOOOooo---